

# Chapter 01 - Earthquakes

M.C. Quigley and B. Duffy

## **A. Learning outcomes**

- *Understand how earthquake fatalities and seismic risk relate to earthquake hazard, exposure and vulnerability*
- *Understand the relationship between tectonic setting, fault type, fault slip rate, and earthquake recurrence interval*
- *Understand the factors that control the amount of fault slip during an earthquake, the moment magnitude of the earthquake, and whether a fault ruptures the surface or not*
- *Understand the different models for earthquake recurrence on faults and implications for the coseismic slip and timing of future earthquakes*
- *Understand the mechanisms by which earthquakes may be triggered*
- *Understand the variety of methods by which earthquakes are measured and characterised*
- *Understand the relationship between fault characteristics (size, kinematics, strength, shape), rupture processes (propagation direction, rupture speed, slip distribution) and earthquake characteristics*
- *Understand the different types of earthquake hazards and how they impact on natural and built environments*
- *Understand the strategies for the assessment, avoidance, and mitigation of earthquake hazards to reduce societal risk*

## **B. Introduction**

Earthquakes and related phenomena such as landslides and tsunami have caused more than 700,000 fatalities, millions of injuries, and more than \$US 700 Billion economic loss since the start of the 21<sup>st</sup> century. With growing population and supporting infrastructure, the world's exposure to natural disasters is inevitably increasing. Some scientists predict that more than 2.5 million earthquake fatalities will occur in the 21<sup>st</sup> century (Holzer and Savage, 2013).

Earthquake fatality catalogues indicate that approximately 75-80 % of earthquake deaths result from the effects of earthquake shaking on the built environment, primarily building damage and collapse (Marano et al., 2010). Tsunami-related deaths (15-20%) and landslide deaths (~5%) contribute the majority of fatalities attributable to natural phenomena (Marano et al., 2010). It is clear that good engineering design, building codes, public education, and land-use planning, informed in part by good earthquake science, have an important role to play in reducing earthquake fatalities. Countries with poor building standards in earthquake prone regions tend to suffer more fatalities when earthquakes occur (e.g. Haiti 2010; < 230,000 fatalities) compared to countries with better building standards (Ambraseys and Bilham, 2011).

The impact of earthquakes on society, typically measured by fatalities, injuries, damage, and economic loss, relates to the spatial and temporal nature of the **earthquake hazard** (e.g., shaking, fault rupture, tsunami, landslide), the **exposure** of humans and their environment to the hazard (e.g., location with respect to strong earthquake shaking, tsunami inundation) and the **vulnerability** of the society and infrastructure to the effects of the earthquake (e.g., building codes, infrastructure resilience). **Seismic risk** (or example the risk of dying in an earthquake or the risk of large financial loss) is the product of hazard x exposure x vulnerability.

The Australasian region is susceptible to earthquake hazards including tsunamis and landslides (Table 1). Parts of Australasia (e.g., New Zealand) have high earthquake hazard but have reduced their vulnerability through science-informed building codes and engineering technologies and practice, and reduced their exposure (in some instances) through land use planning decisions. Other parts of Australasia (e.g. Australia) have lower earthquake hazard but higher vulnerability due to lower seismic building codes, such that a 'rare' earthquake could inflict significantly more damage than an equivalent event in New Zealand. Other parts of Australasia have high hazard, high exposure and high vulnerability (e.g. Papua New Guinea); in such environments earthquakes pose a major risk and have the potential to cause large numbers of fatalities (Table 1).

This purpose of this Chapter is to provide information on the origin of earthquakes, the relationships between earthquakes and fault processes, how earthquakes are measured and documented, and the controls on the nature and distribution of earthquake hazards. A particular emphasis is placed on earthquake science within the context of Australasia. We conclude with a New Zealand-based case study and some review and discussion questions. Detailed descriptions of important terms (typically appearing in **bold text**) and other information relating to this chapter appear in the on-line Glossary and Supplementary Information available at [XXX.cambridge.org](http://XXX.cambridge.org).

## **C. The Origin of Earthquakes**

### *C.1. Plate tectonics, stress, and rock fracturing*

We live upon a restless planet. The tectonic plates that comprise Earth's rigid outer shell are in constant motion, moving in different directions at different velocities. The Australasian region includes two of Earth's fastest moving plates, the Australian and Pacific Plates (Figure 1A), which move at velocities of up to 70 mm per year, roughly twice as fast as your fingernails grow. The Antarctic Plate is one of the slowest moving plates on Earth, moving < 10 mm per year (Figure 1A). Tectonic plates consist of continental and / or oceanic crust and underlying mantle. The combined thickness of crust and lithospheric mantle typically ranges from 80 to 200 km. The processes that control the direction, rate, and types of tectonic plate movement are summarized in the Supplementary Information accompanying this chapter.

The Earth's lithosphere is riddled with fractures of all sizes, dimensions, and orientations. This is particularly the case for continental crust, much of which has been fractured and deformed for millions to billions of years as it has traversed the globe. Forces generated at plate boundaries and within plate interiors influence both the direction and magnitude of **stress** (i.e. **stress vectors**) acting on a given fracture. When the maximum **shear stress** exerted on fracture plane exceeds the frictional strength of the fracture, the fracture may break and displacement may occur. Where displacement occurs, this is termed a **fault** (Figure 2). If displacement on a fault occurs rapidly, it

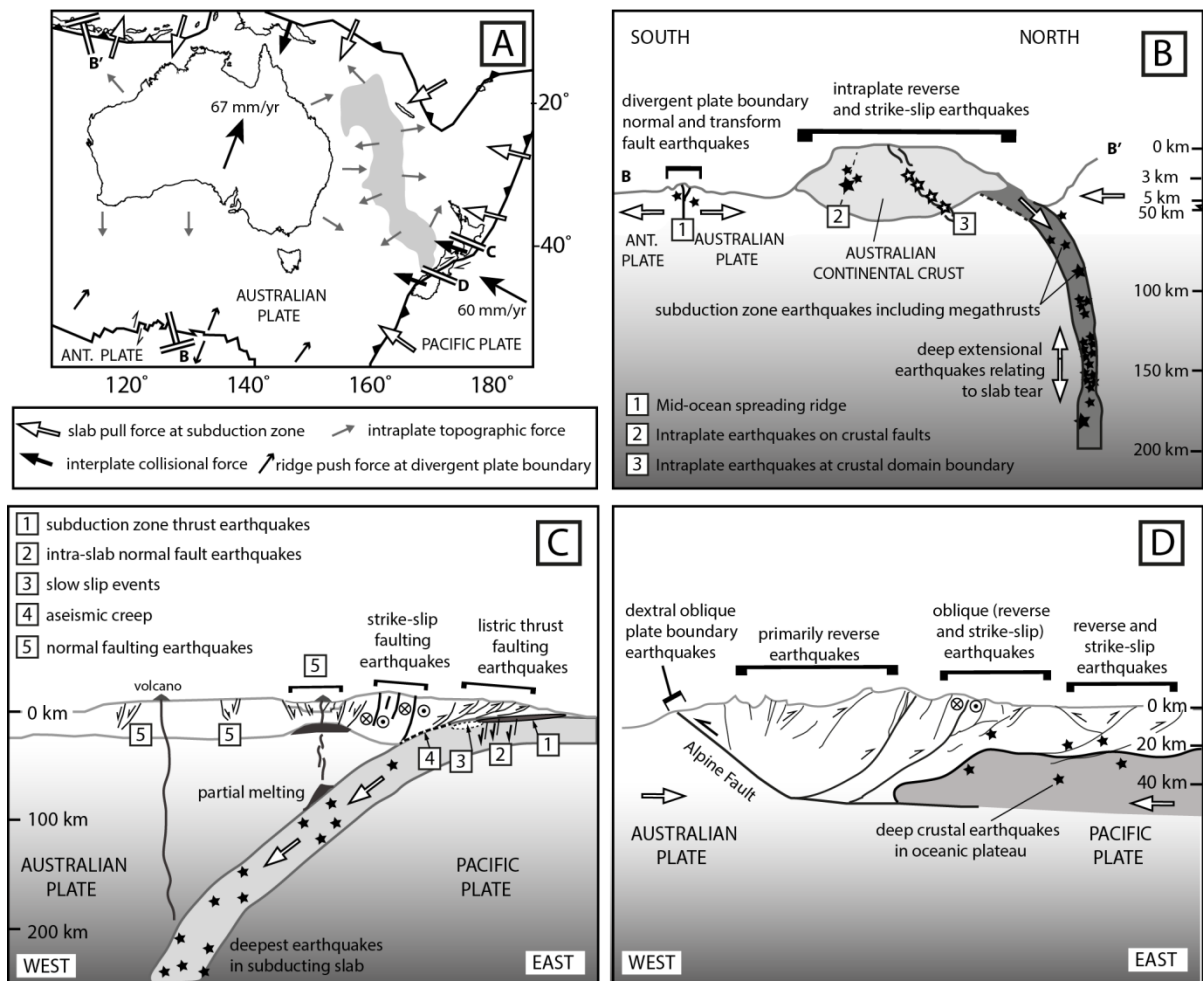


Figure 1

**Figure 1.** A) The plate tectonic setting of Australasia, spanning the Australian, Antarctic (ANT) and Pacific tectonic plates. Plate motion vectors shown for the Australian and Pacific Plates. Forces driving and resisting plate motion, and acting on the plate boundaries and within plate interiors, as shown by small arrows. Location of sections B-D as shown.

B) Cross-sectional cartoon through the Australian plate, from the southern divergent plate boundary to the northern subduction plate boundary. Locations and depths of different types of interplate and intraplate earthquakes as shown; note that depths are not to scale (crustal part of section is depth-exaggerated).

C) Cross-sectional cartoon through the Australian-Pacific plate boundary in New Zealand's North Island, showing the variety of tectonic processes and related locations and types of earthquakes associated with subduction.

D) Cross-sectional cartoon through the Australian-Pacific continent-continental collisional plate boundary in New Zealand's South Island. Note the reverse in subduction zone polarity between C and D. Types and depths of earthquakes as shown. See Section B for details.

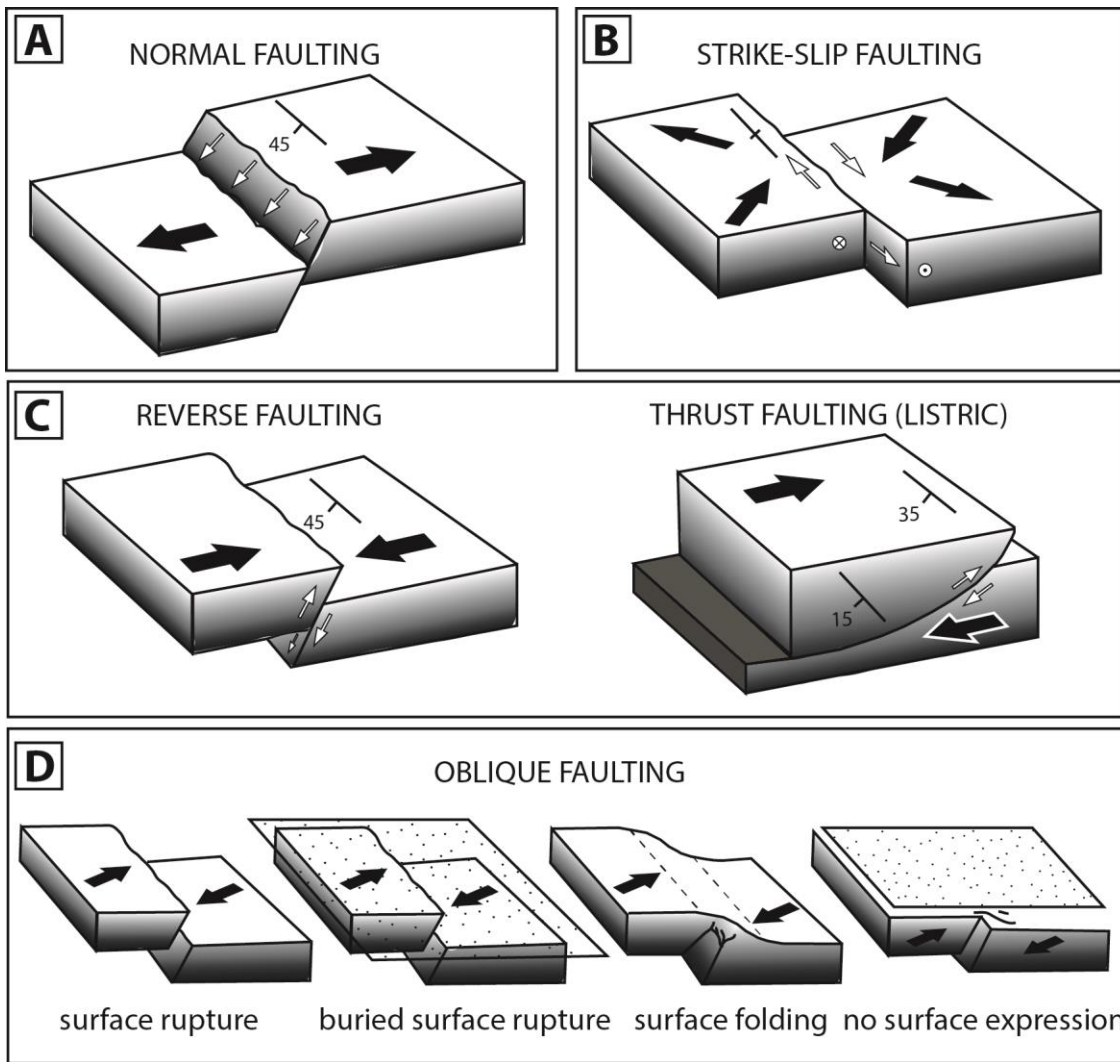


**Figure 2.** Types of faults. Black arrows show relative motions of adjacent fault blocks. White arrows show direction of fault slip. Strike and dip symbols show fault orientation. Relationships of faulting to surface expressions shown in Panel D. Faults with surface folding but no evidence for discrete surface rupture, or no surface expression of folding or faulting, are referred to as 'blind' faults.

**Table 1.** Notable earthquakes in Australia and New Zealand, sorted by date. This list is far from comprehensive but serves to show that every state or region of Australia and New Zealand has experienced earthquake activity during the history of European settlement.

Region	Date	M <sub>w</sub>	Deaths	Injuries	Comment
<b>Australia</b>					
VIC	1885-07-03	5.7			Victoria's joint largest earthquake. Minor damage but widely felt
SA	1897-05-10	6.5		>5	Several serious and numerous minor injuries. Severe damage to homes, buildings, power lines, and railways.
WA	19/11/1906	7.8			Indian Ocean event - knocked bottles off shelves in Perth
TAS	29/12/1929	5.6			Significant damage in Launceston, Tasmania, felt across Western Tasmania
QLD	12/04/1935	5.5	1		Considerable damage in Gayndah, 52 years after similar event.
WA	14/10/1968	6.7		20	Meckering. Rupture of 35 km long reverse fault. 60 buildings destroyed. Minor damage in Perth. Total damage \$5 million.
SA	30/03/1986	6			Rupture produce a 13 km long surface trace with a maximum displacement of 0.6m
NT	22/01/1988	6.7			Tennant Creek NT; Two buildings and 3 other structures damaged, damage caused to natural gas pipeline. Total damage \$2.5 million.
NSW	28/12/1989	5.7	13	160	Newcastle earthquake. 1.1 billion \$ damage MM VIII in the Newcastle area. Felt over 200,000 km <sup>2</sup> .
NT	11/12/2012	7.1			Banda Sea earthquake, felt in Darwin
<b>New Zealand</b>					
MBo	16/10/1848	7.8	3		1848 Marlborough earthquake on dextral Awatere Fault. Deaths occurred during aftershock.
Wai	23/01/1855	8.2	9	5	1855 Wairarapa earthquake. Numerous landslides occurred, and up to 6 m of uplift.
Akl	23 Jun 1891	5.5-6.0			Waikato Heads earthquake caused MM5-6 shaking in Auckland
Cant	16/11/1901	6.8	1		1901 Cheviot earthquake
WC	17/06/1929	7.8	17	1	1929 Murchison earthquake. 14 deaths were landslide-related, 2 were coal miners. No aid for 2 weeks, no vehicle access for several months. 4.5 m vertical and 2.5 m lateral displacement
HB	3/02/1931	7.8	256	593	1931 Hawke's Bay earthquake. Total devastation caused 1000s of minor injuries.
Wai	1/08/1942	6.8	1		August 1942 Wairarapa earthquake. Late night timing saved lives in Wellington, which was badly damaged. 1 death due to fractured gas pipe.
Cant	26/06/1946	6.2			Lake Coleridge earthquake. Earthquake 21km from Lake Coleridge caused landsliding below the lakes surface, close to a major hydro-electric power station.
WC	24/05/1968	7.1	2	?	1968 Inangahua earthquake. Lack of communications delayed widespread knowledge of the earthquake by several hours.
BoP	2/03/1987	6.5		25	1987 Edgecumbe earthquake
BoP	20/12/2007	6.6			2007 Gisborne earthquake – offshore, >\$30M losses
SL	15/07/2009	7.8			2009 Fiordland earthquake
Cant	4/09/2010	7.1			2010 Darfield earthquake. No deaths, few injuries. 30 km rural surface rupture
Cant	22/02/2011	6.2	185	220	February 2011 Christchurch earthquake. >6000 minor injuries.
MBo	16/08/2013	6.6		4	2013 Lake Grassmere earthquake. Mainshock and aftershock

## Abbreviations:

NSW – New South Wales; NT – Northern Territory; QLD – Queensland; SA – South Australia; TAS – Tasmania; VIC – Victoria; WA – Western Australia

AKL – Auckland; BoP – Bay of Plenty; Cant – Canterbury; HB – Hawkes Bay; MaW – Manawatu; MBo – Marlborough; SL – Southland; Wai – Wairarapa; WC – West Coast

---

---

sends out energy waves that are defined as an **earthquake**. Almost all earthquakes involve **shear displacement on a pre-existing fault**; very few earthquakes are thought to originate from new faults in unfractured rock. The process of fault slip causing an earthquake is typically referred to as **fault rupture**.

### *C.2. Earthquakes, faults, and plate tectonic settings*

The five main types of faults can be classified by the direction of fault slip with respect to the dip of the fault (Figure 2). Definitions of **normal, thrust, reverse, strike-slip, and oblique faults** are provided in the Glossary and Figure 2 caption.

The amount of fault slip in an individual earthquake (i.e. **coseismic slip**) is typically only a very small increment of the total amount of slip accumulated on the fault over its history; most faults evolve as a result of hundreds to thousands of earthquakes incurred over millions of years. However, the direction of fault slip in a large individual earthquake is typically consistent with the average orientation of the fault slip deduced from geologic studies of the geologically recent (e.g. Quaternary) behaviour of the fault. As such, geologic studies of faults (i.e. fault paleoseismology) provide us the opportunity to (1) learn about past earthquakes, (2) determine the likely orientation of contemporary stresses, and (3) forecast the timing, direction and amount of slip in future earthquakes. In general, most earthquakes will occur due to crustal extension within normal fault zones, crustal contraction within reverse and thrust fault zones, and lateral shearing within strike-slip fault zones. Important concepts including **fault inheritance, fault reactivation, fault kinematics, and stress fields** are discussed in the Glossary.

Active faults in New Zealand have **earthquake recurrence intervals** ranging from < 300 years and **fault slip rates** > 20 mm per year (e.g., Alpine Fault; Berryman et al., 2012) to > 20,000 years and < 1 mm per year (e.g., Greendale Fault – the source of the 2010 Darfield earthquake in New Zealand; Hornblow et al., 2014). Some faults responsible for historical earthquakes may have recurrence intervals more than 50,000 years and slip rates less than 0.1 mm per year but are still demonstrably tectonically active (e.g. Lake Surprise Fault – the source of the 1988 Tennant Creek earthquake in Australia's Northern Territory – see Table 1) (Crone et al., 1997). Interestingly, some active faults in arid intraplate interiors like Australia, with long recurrence intervals (>30,000-100,000 years) and low slip rates (<0.1 mm per year), may still be active enough to build mountainous topography, steep relief and strongly influence erosion rates (Quigley et al., 2006, 2007a,b, 2010). If an identified fault has not had any major earthquakes on it during the Quaternary period (~2.6 million years ago to Present) it may be reasonably classified as an **inactive fault**, although proving a fault is incapable of generating future earthquake is typically quite challenging!

The amount of fault slip that occurs in an earthquake relates to the **area of the fault rupture**, which, for simple fault geometries, can be estimated from the **fault subsurface rupture length** and **down-dip rupture width** (Figure 3A). The latter is limited by the thickness of the brittle crust and the dip of the fault, so that vertical faults may have smaller down-dip rupture widths than inclined faults. The **moment magnitude of the earthquake ( $M_w$ )**, which is a measure of earthquake energy, is proportional to both the amount of coseismic slip and the rupture area (Figure 3, 4). Not all earthquake ruptures encompass the entire extent of an identified fault. There is a wealth of studies focused on understanding why some earthquakes involve the entire fault area (i.e. 'wall-to-wall' ruptures) whereas some earthquakes involve a smaller area of the total fault (i.e. 'segmented' ruptures) (e.g., Wesnousky, 2008). For the most part, longer faults have longer maximum rupture lengths and areas, greater coseismic slips, and higher  $M_w$  potentials than shorter faults.

Factors such as the geometry and size of the fault rupture, the amount and direction of fault slip (**rupture propagation direction**), the nature of the faulted materials, and the geologic and geomorphic setting of the fault will collectively influence whether the fault ruptures through to the Earth's surface (Figure 2D, Figure 3A). Faults with enough displacement may cause a **surface rupture**. Some surface ruptures may be subsequently **eroded** or **buried**, thereby obscuring or removing surface evidence of faulting and making their detection based on surface studies more difficult (Figure 2D). Earthquakes on other faults may cause folding or doming of the Earth's surface without causing a discrete surface rupture (Figure 2D). Some faults may not have sufficient slip to influence the topography at the Earth's surface at all. Faults that do not rupture the surface are referred to as **blind faults** (Figure 2D). For every large fault we can map on the surface, there are likely to be 10's to 100's of smaller blind faults that contribute to seismic hazard.

The shapes of earthquake ruptures on faults may be irregular, but are often approximated by an ellipse (Figure 3A). The geometric centre of a fault rupture is typically referred to as the **centroid** (Figure 3A). The area of the fault where the rupture begins is called the **hypocentre** or **focus** of the earthquake; this spot can be defined in terms of its geometric co-ordinates (x,y) and its **hypocentral depth** (z). The point on the earth's surface immediately above the hypocentre is called the **epicentre**. During an earthquake, the rupture typically propagates along the fault outward in all directions, although some ruptures propagate primarily in one direction (**unilateral ruptures**) and some propagate in different directions (**bilateral ruptures**). Typical rupture propagation speeds range from 1 to 3 km per second. Thus for the same fault rupture area and rupture velocity, the duration of a perfectly unilateral rupture would be twice as long as a perfectly bilateral rupture. The area of maximum slip on a fault may not be in the same place as the hypocentre, epicentre, or fault centroid. For most continental earthquakes, the most amount of slip tends to occur in the central parts of the fault at depths of 3-6 km. Information about seismic data is used to determine the hypocentre location and kinematics of an earthquake is provided in the Supplementary Information.

Major continental faults are not simple planar features confined to one surface; rather they are zones of highly fractured rock that are commonly wider than 100 m, and even wider than 1 km (Figure 3B). Fault zones typically consist of a **principal slip zone** that may result in a **surface fracturing zone**, flanked by a **zone of surface deformation** within a region of **wall rock**.

The nature of the **tectonic plates** and their relative movement exerts the strongest influence on the types of earthquakes that occur. See Figure 1 and the Supplementary Information section for a

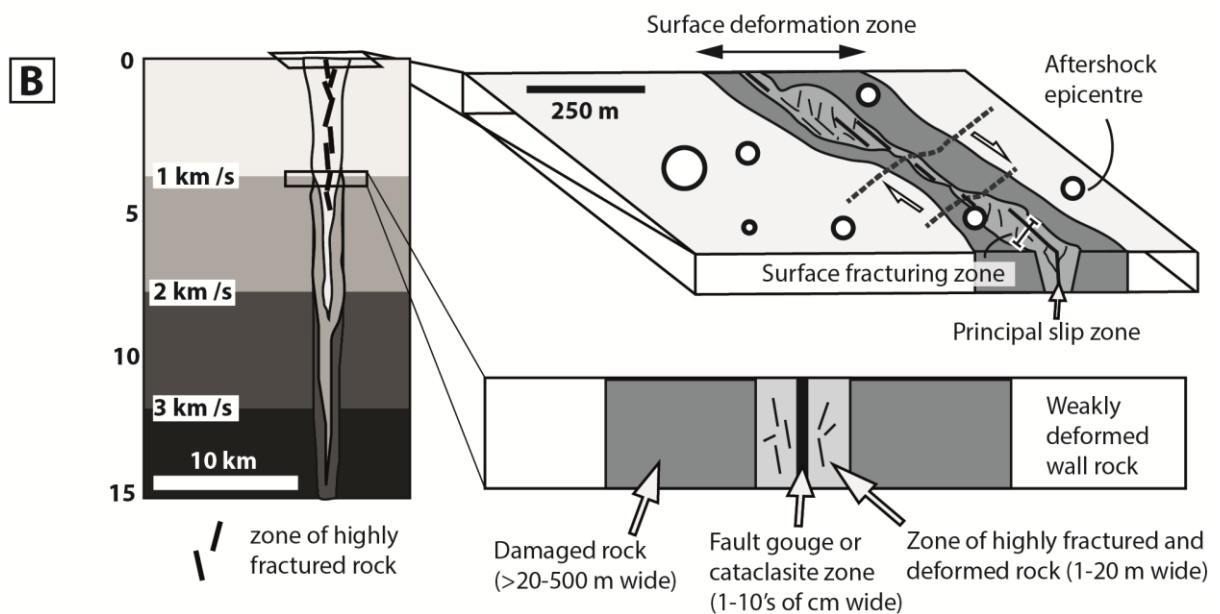
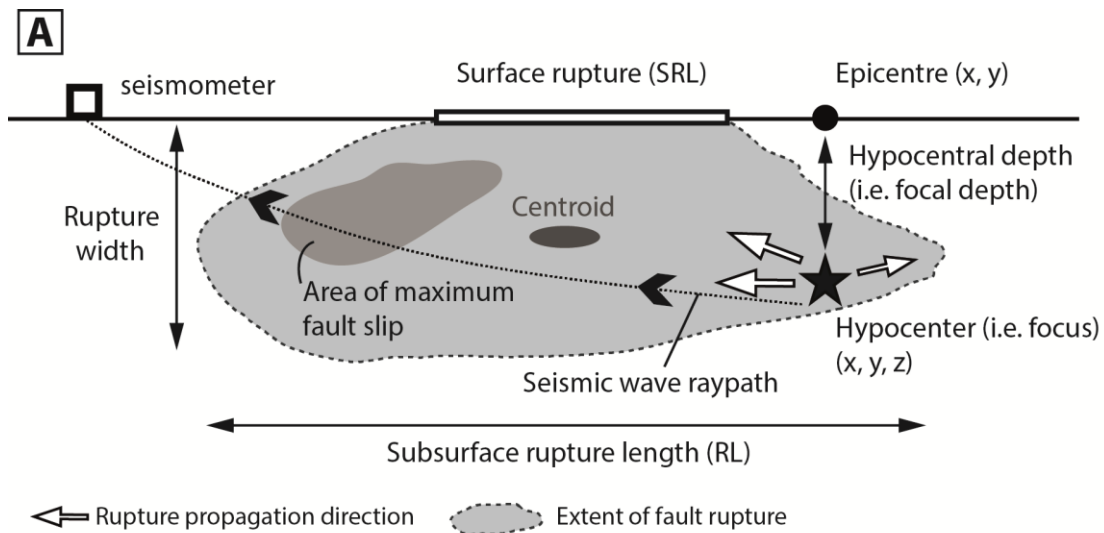


**Figure 3.** A) The subsurface anatomy of an earthquake rupture, viewed perpendicular to the fault plane. Descriptions of labelled features appear in Section B.2. Note discrepancy in the location of the hypocentre, centroid, and area of maximum slip. This rupture would be classified as unilateral (hypocentre located at one end of the fault, rupture propagation primarily in one direction). Not irregular shape of rupture extent. Hypothetical seismic wave ray path initiating from hypocentre and arriving at nearby seismometer as shown.

B) Cross-sectional depth profile of a fault zone and related changes in seismic shear wave velocities that reflect the geometry and width of damaged rock associated with fault rupture. Image modified from Li et al. (2014). Blow up images show fault surface and subsurface deformation zones. See Section B.2 for more details.

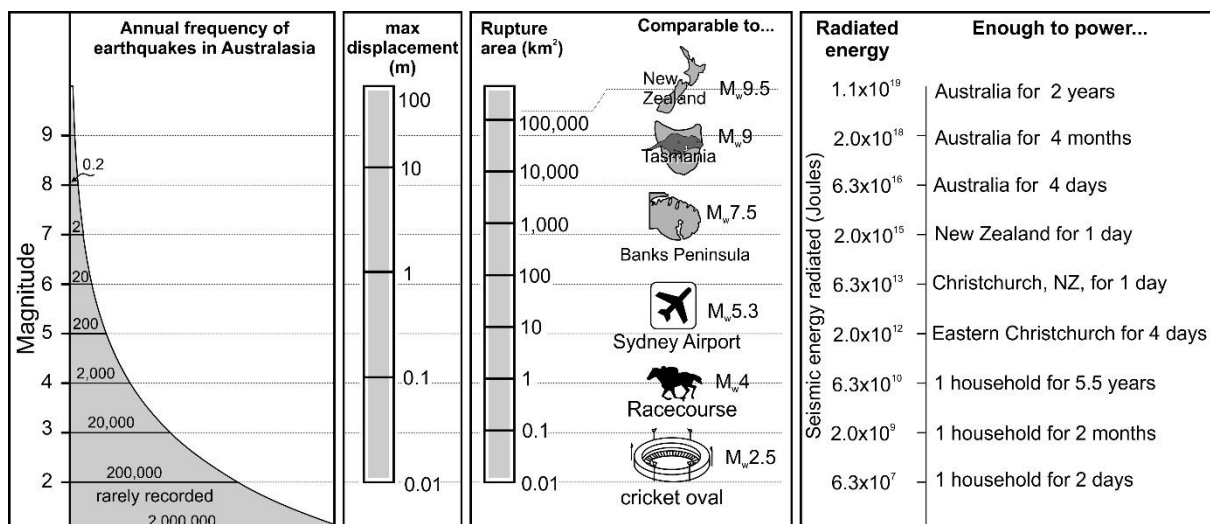


**Figure 4.** Scaling relationships between earthquake moment magnitude and frequency in Australasia, displacement, rupture area and radiated energy. Rupture areas are compared to well-known landmarks of different sizes. Radiated energies in Joules are translated into power usage metrics. The ‘Australasia’ region spans from Bali, to Fiji, to the Auckland islands, to the southwest corner of Australia.

summary of **divergent, convergent, and strike-slip plate boundaries** and tectonic controls on the characteristics of earthquakes.

## **D. Earthquake behaviour and triggering**

### *D.1. Models for describing earthquake behaviour*

The stress acting on a fault plane increases over the **interseismic period** (i.e. the time period between successive major earthquakes) due to tectonic plate movement, which causes slow, continuous differential movement of rocks on either side of the fault (Figure 5A). If fault remains **locked** (i.e. does not slip), then broad deformation may occur around the fault due to the relative motion of the adjacent rocks. This deformation is stored within the rocks in the form of **elastic shear strain**, which can be envisaged as the bending of a formerly straight feature across the fault zone. The term elastic is used because this deformation is recoverable, rather than permanent. Elastic strain increases throughout the interseismic period in the absence of fault slip (Figure 5A).

Once the stress on the fault increases to a level in excess of the **frictional strength of the fault** (i.e. **failure stress**), fault rupture occurs. During the earthquake rupture (i.e. **coseismic**) the stress state on the fault drops rapidly (i.e. **stress drop**; Figure 5B), and the elastic strain is converted into permanent strain in the form of **fault displacement**, resulting in an elastic strain decrease (Figure 5C) and total fault displacement increase (Figure 5D). If all of the accumulated elastic strain is converted to permanent strain, then formerly straight features perpendicularly crossing the fault may return to their same orientations, although they will be displaced (Figure 5A–Panel 4). Stress may continue to dissipate and / or be redistributed on the fault immediately following the earthquake (i.e. **post-seismic**), and may be accompanied by a reduction in elastic strain and continuation of slow postseismic displacement on the fault (Figure 5B to 5D). The time encompassing the coseismic, postseismic, and interseismic intervals between successive earthquakes is termed the **earthquake cycle** and it is underpinned by the **elastic rebound theory** (Reid, 1910) (Figure 5A).

If the rate of stress accumulation on the fault (i.e. **stress loading rate**;  $\sigma_{Lr}$  in Figure 5E), the frictional strength of the fault (equivalent to failure stress,  $\sigma_F$  in Figure 5E), and the stress drop ( $\Delta\sigma$  in Figure 5E) associated with each earthquake is constant throughout the earthquake cycle, then earthquakes should occur at regular time intervals ( $\Delta t$ ) and with consistent fault slip. In this case, one could **predict the timing, slip, and  $M_w$  of future earthquakes** based on the timing and slip of previous ones. This model for earthquake recurrence is called the **periodic earthquake model** and is shown by earthquakes 1-3 in Figure 5E. Earthquake 3 was preceded by some small earthquakes ('i' in Figure 5E; termed **foreshocks**), but these made little difference in the recurrence interval. Sometimes earthquakes may occur at lower (e.g. earthquake 4) or higher than expected failure stresses. In the case of earthquake 4,  $\Delta t$  was shorter than prior events, however the stress drop returned the stress state on the fault back to the same **residual stress** level ( $\sigma_R$ ) as earthquakes 1 to 3. This represents an example of a **slip-predictable earthquake**; the amount of stress drop and associated fault slip of the forthcoming earthquake can be predicted based on the time elapsed since the last earthquake, however the timing of the forthcoming earthquake is unknown. Sometimes earthquakes fail at the expected failure stress but have lower than expected stress drop (e.g. earthquake 5). This is an example of a **time-predictable earthquake**; the timing of forthcoming earthquake can be predicted from the timing and slip of the last earthquake because the seismic loading rate is constant, however the slip in the forthcoming earthquake is unknown.

If the stress loading rate between earthquakes varies with time (e.g., ii, iii) then the timing of the next earthquake may not be predicted, even if the failure stress is similar to preceding earthquakes (e.g. earthquake 6). Increases or decreases in stress loading rate could reduce or increase the time to the forthcoming earthquake. Furthermore, continued slip after the expected coseismic stress drop (e.g. iv) could increase the time until the forthcoming earthquake. An overall stress loading rate might experience step changes (e.g., v) due to, for instance, earthquakes on other nearby faults (open stars) that increase the stress on the fault of interest; such step change increases bring forward the time of the forthcoming earthquake (earthquake 7). A stress drop following an earthquake might be similar to preceding earthquakes but accomplished in a different fashion, for instance by a cluster of smaller earthquakes, rather than a single event (small stars, vi).

Detailed descriptions of earthquake physics are rupture behaviour are provided by Scholz (1992) and Kanamori and Brodsky (2004) amongst many others. Clearly, earthquake patterns on individual faults are not so simple, although some faults may behave more regularly than others (Berryman et al., 2012). Perhaps one of the reasons for why earthquake recurrence doesn't seem to keep on a tight schedule relates to the myriad of ways in which earthquakes may be triggered.

#### *D.2. Earthquake triggering*

Understanding the processes that cause an earthquake (i.e. earthquake triggering) is important, because many recently damaging earthquakes (e.g., 2011 Christchurch earthquake) were almost certainly triggered by preceding events (e.g., 2010 Darfield earthquake). Earthquakes can be triggered by a variety of processes (Figure 6). The majority of earthquakes occur because tectonic forces have increased stresses in the vicinity of faults to a level where they exceed the frictional strength of the fault, resulting in failure and the generation of earthquakes. However, it seems that a lot of faults exist at high levels of differential stress, waiting to spring into action when small perturbations to local, regional or even global stress fields encourage them to. These changes in

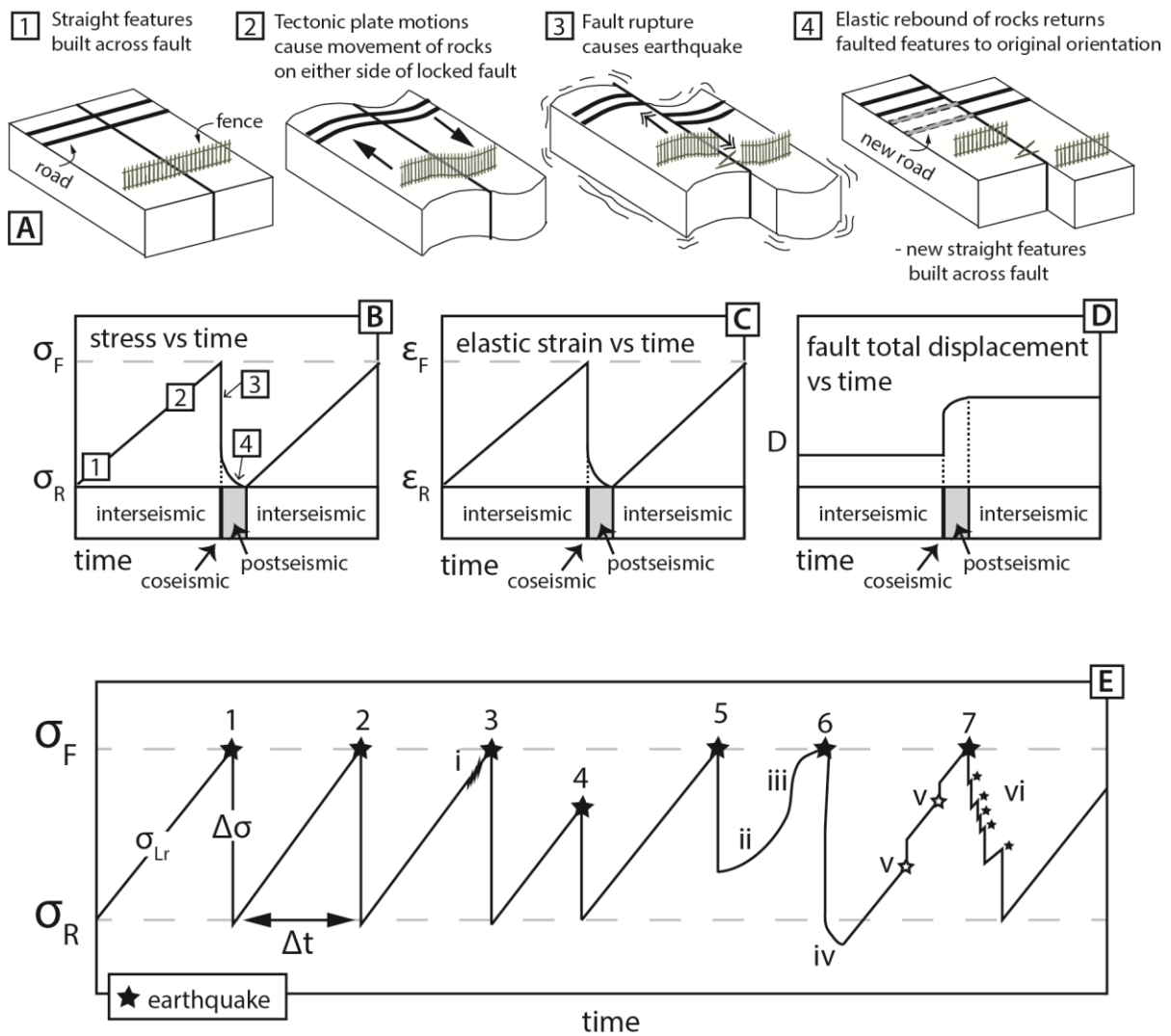


**Figure 5.** A) The seismic cycle and elastic rebound, as initially posed by Reid (1910). Straight features across a fault (1) are slowly bent (2) as fault blocks experience relative movement across a locked fault in the interseismic period. During fault rupture (3) displacement occurs across the fault, and formerly straight features are returned to their initial orientations (4), although they are displaced across the fault.

B) Plot of fault stress vs time through the seismic cycle. Boxed numbers correspond to the sequence in part A. Stress on the fault builds from a residual level ( $\sigma_R$ ) to a failure level ( $\sigma_F$ ), at which stage fault rupture occurs. Coseismic stress drop may return the fault to the residual level, or further stress decrease may occur via postseismic deformation.

C) Elastic strain versus time through the seismic cycle. Elastic strain in the rocks surrounding the fault increases in the interseismic period and decreases co- and postseismically.

D) Fault total displacement versus time through the seismic cycle. For a locked fault, no displacement occurs during the interseismic cycle. Elastic strain is transformed to permanent displacement during the earthquake. Some further deformation may occur in the postseismic period.

E) Stress evolution during characteristic (1,2,3) and non-characteristic (4-7) earthquakes. See Section B.5 for details.

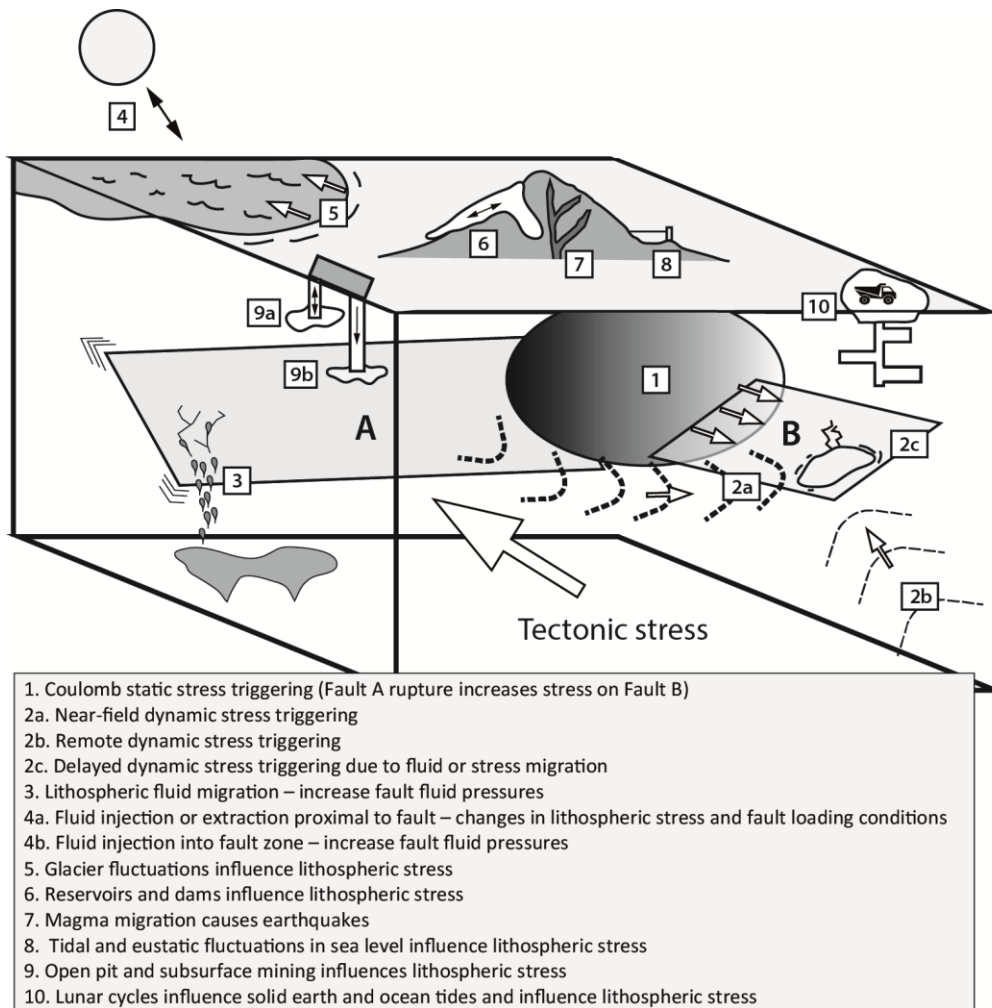


**Figure 6.** The many ways in which earthquakes may be triggered.

stress may be **induced by slip on other faults**, which changes the shape of the crust and corresponding stress field around that fault ('1' in Figure 6). If the change in stress field encompasses other faults, those faults may experience an increase (or decrease) in the applied stress. Scientists call this a **Coulomb static stress change**, and it is now a well-recognized process for triggering earthquakes (King et al., 1994). Earthquakes may also be triggering by **dynamic stresses** associated with the passage of seismic waves from other earthquake sources through the fault zone (Kilb et al., 2000). This may occur due to earthquakes on nearby faults ('2a' in Figure 6) or more distal faults ('2b' in Figure 6). Dynamic stresses might immediately trigger seismicity, or might induce processes such as microcracking and fluid migration, that ultimately trigger an earthquake some time long after the seismic waves have passed ('2c' in Figure 6). The **migration of fluids** sourced from great depth through the lithosphere may increase the pore fluid pressure in fault zones, thereby triggering earthquakes ('3' in Figure 6).

A variety of natural and anthropogenic processes operating near or at the earth's surface influence lithospheric stress, and may thus trigger earthquakes. Changes in the position and distance of moon relative to the Earth influence the direction and magnitude of **tidal stresses** – this includes both the shape of the Earth (**solid Earth tide**; '4' in Figure 6) and the extent and magnitude of **ocean tides** ('5' in Figure 6). Solid earth and ocean tidal fluctuations may induce small stress changes on faults and, under the right circumstances, might trigger earthquakes. Over significantly longer timescales,

**eustatic changes in sea level** ('5' in Figure 6) also influence lithospheric stresses and could be considered as a possible triggering mechanism for earthquakes. Fluctuations in the extent and volumes of **glaciers** may influence the load on the crust and consequently the stress field around faults, thus influencing earthquake occurrence ('6' in Figure 6). Both natural and anthropogenically influenced changes in **surface hydrology**, such as natural and dammed lakes, may influence crustal stresses and effect **subsurface hydrology** near fault zones, thereby influencing earthquake occurrence ('7' in Figure 6). **Magma and/or fluid migration** in volcanic systems may also trigger earthquakes ('8' in Figure 6). The **injection or extraction of fluids** may change the stress field around fault zones and thus trigger (or inhibit) earthquakes ('9a' in Figure 6). The **injection of fluids** into fault zones may help to **lubricate** them via changes in the fluid temperatures and pressures and trigger earthquakes ('9b' in Figure 6); this phenomenon forms the basis for **fracking**. The excavation of rock in **open pit and subsurface mines** ('10' in Figure 6) may also influence the surrounding stress field and influence earthquake occurrence.

It is important to recognize that earthquakes have occurred over billions of years on planet Earth. While anthropogenic activity may have an influence on the locations, rates, and types of earthquakes in some circumstances, earthquakes have been a natural occurrence long before any human influence. We are virtually certain that almost every large fault that has hosted a major historical earthquake has had many earthquakes prior to the relatively short time over which humans have been observing and recording earthquakes, and influencing the subsurface with our activities. A discussion on **earthquake forecasting, earthquake predictions and earthquake precursors** is provided in the Supplementary Information section.

## **E. Measurement and characterisation of earthquake shaking and faulting**

### *E.1. Earthquake shaking intensity*

An earthquake is commonly felt most intensely closest to the earthquake source rupture. Shaking intensity typically decreases with increasing distance from the source fault. This is because seismic wave amplitude typically declines with distance as wave energy passes through an increasingly large volume of earth. The human perception of shaking intensity is related to the effects we feel, such as falling, and observe around us during shaking, such as the nature and scale of damage to human constructions such as buildings, roads, and bridges. This led to the early 20<sup>th</sup> century development of **felt intensity** scales, which allow scientists to assign a numeric intensity value based on descriptions of earthquake experiences, and facilitate comparison between sites and between earthquakes. With online felt intensity reporting, the data generated by the public can be considerable. Intensity values can also be retrospectively assigned to localities based on published accounts of historic earthquakes.

The most commonly used scale is the **Modified-Mercalli Intensity (MMI) scale**, a twelve-stage scale that ranks effects between barely perceptible shaking (MMI I) and total destruction (MMI XII). MM IV is the lowest intensity that is widely felt. Intensity reports are typically displayed on a shaking intensity map, on which contours called **isoseismals** join points of equal MMI intensity. The shape of isoseismals provides an indication of both size and location of shallow earthquakes, as well as highlighting the worst-affected areas. The 'bulls-eye' of highest MMI values is often interpreted to mark the earthquake epicentre, although this is undoubtedly a simplification.

The intensity of earthquake shaking at a site may be measured using an **accelerometer**, which records acceleration relative to gravity using three orthogonal sensing heads. Similar devices are found in most phones and tablet computers, where they sense orientation of the device and let you see your pictures the right way up, as well as correcting for shaky hands whilst taking photographs. Unlike seismometers, accelerometers are not continuously recording and must be triggered by **strong ground motion**.

The most important characteristics of strong ground motion are the **duration, intensity (wave amplitude, velocity, and acceleration), and frequency content of shaking**. The duration of shaking above a certain intensity value often relates to the severity of damage experienced in natural and built environments. The amplitude of the surface waves (half the size of the wave from peak to trough) provides a measure of the displacement of particles on the surface of the earth. Typical amplitudes are less than 10 cm, though ground displacements at low frequencies may reach 1m or more in large earthquakes. Ground displacements with respect to time (including **peak ground displacements, PGDs**) can be used to calculate the **peak ground velocity (PGV)**, which describes the maximum speed at which the ground particles move. This can be broken into horizontal (PHV) and vertical components (PVV). The direction and speed of movement is always changing, both horizontally with the passage of Love waves, and vertically with the passage of Rayleigh waves. The maximum rate at which these velocity changes occur is expressed as the **peak ground acceleration (PGA)** and is commonly reported as a fraction of the acceleration of gravity (e.g., % g). PGA may also be described in terms of horizontal (PHA) and vertical components (PVA). The displacement, velocity, and acceleration are different measures of earthquake shaking intensity.

The **frequency content** of strong ground motion (how amplitude is distributed amongst different frequencies) is an important measure of earthquake shaking. An earthquake generates a range of frequencies of seismic waves (from high to very low frequency). The frequency content is generally related to magnitude, with larger earthquakes generating more low frequency waves. The ground acceleration generated during the passage of seismic waves causes most of the coseismic damage to structures. Peak ground acceleration at a specific site occurs at a specific, typically high, frequency. Peak ground velocity typically occurs at lower frequencies than peak ground acceleration, so what parameter better predicts the damage due to an earthquake? The answer lies in the tendency of buildings to resonate, i.e. oscillate with greatest amplitude at a specific frequency.

The inverse of frequency is called the period (T) of a wave (the time between the passing of two consecutive wave crests). The **resonant frequency** of buildings can be approximated as a period of 0.1s per storey of building. So, taller buildings have a longer natural period, and resonate at lower frequencies. Buildings are most susceptible to damage when subjected to large amplification of waves at their period. High frequency, short period motions applied at the base of a tall structure will cause little rocking of the structure. However, large, low frequency, long period motions at the base of the same structure will cause rock alarmingly. This gives rise to the concept of **spectral acceleration (SA)**, which is a way of quantifying the acceleration at a certain frequency. SA is often reported at values of the natural period of vibration for buildings to assist in defining building codes and assessing vulnerabilities of buildings to different frequencies and intensities of seismic shaking.

The amount of coseismic slip, fault surface roughness, dynamics of the rupture process, and direction in which an earthquake rupture propagates (**rupture directivity**) all influence the

characteristics of the earthquake, typically referred to as **source effects**. The **lithospheric structure and composition** between the source and the felt area influence how seismic energy is attenuated (**path effects**). The topography and geology at the site of interest (**site effects**) also influences the duration, frequency content, and intensity of seismic shaking. The concepts are explored in more detail in the Supplementary Information section.

## *E.2. Measuring fault ruptures*

Historic surface ruptures are typically documented to determine or estimate the surface rupture length, vertical and horizontal displacement profiles, and width of the zone of deformation (Figure 3). At the largest scale, **interferometric satellite altimetry radar (InSAR)** has been used since the mid-1990s to document surface deformation at centimetre scale (Figure 7). A satellite flying across the sky looks sideways and down in a given direction (the look direction) and records the distance to each point on the ground surface, producing a **satellite altimetry radar (SAR)** image. A repeat survey after an earthquake can be correlated with the original data to produce an **interferogram**, which records the deformation as a series of fringes, each representing an increment of displacement relative to the satellite. A continuous regional deformation field is developed by summing and interpolating between deformation fringes. However, interferograms commonly lose coherence close to the fault trace, where most of the deformation is concentrated. They also lose coherence if there is an excessively long time gap between acquisition of pre and post-seismic imagery. In a similar way to InSAR, other multi-temporal optically sensed imagery, including **satellite and aerial photography**, can be orthorectified and coregistered, allowing sub-pixel correlation of the images to measure ground deformation.

**GPS** (US owned) or Global Navigation Satellite System (**GNSS** – multinational) surveys (Figure 7) may be re-occupied after an earthquake to obtain high resolution determinations of their new 3d coordinates. Coseismic deformation may then be calculated from pre to post-seismic changes. As with InSAR, these surveys show regional deformation patterns but in most cases do not yield high resolution data close to the fault.

One of the most rapidly growing tools for documenting earthquake surface ruptures is **airborne or terrestrial light detection and ranging surveys (LiDAR)**. The LiDAR instrument scans a swath of the ground surface to determine the distance to the ground (Figure 7). A digital topographic model is then developed that is tied to an appropriate coordinate system. Most surface ruptures are now quickly surveyed with a combination of LiDAR and co-registered aerial photography. These are high cost techniques but airborne LiDAR is capable of providing high resolution topographic data at 0.5 m resolution over large distances, usefully filling areas of incoherence in InSAR surveys. The technique is especially useful in thickly vegetated areas (e.g., De Pascale et al., 2014), where only a few laser impulses might be able to reach the ground. High density surveys can be filtered to select only the last return from a given area, which is usually the ground surface below the canopy. Many regional authorities use LiDAR surveys for planning purposes, particularly in floodplains. This growing coverage of existing LiDAR surveys is providing opportunities to difference pre and post seismic topography and obtain models of surface deformation with resolution of approximately 10 cm.

Following an earthquake, a surveyor may re-occupy the boundary marks that define a deformed property and determine how the shape has changed. These surveys, called **trilateration surveys** (Figure 7), can help to define the shape of the incremental strain ellipse. Cadastral-type surveys

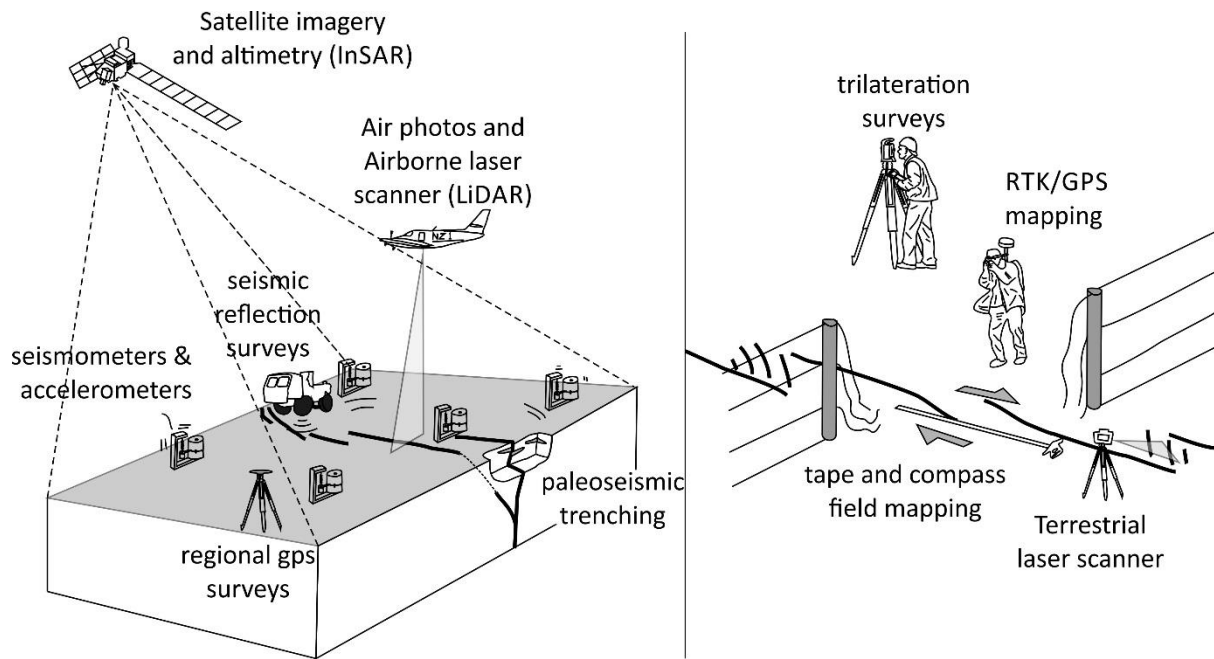


**Figure 7.** Methods for measuring earthquake ruptures and studying active faults. See Section C.7 for detailed descriptions.

provide relative displacement data at cm-resolution (compared with 0.5 m resolution LiDAR models), and at a range of distances from a fault. They provide useful infill of near fault data, compared with InSAR and regional GPS, and can help to define fault geometry and slip distribution with depth.

Ultimately, the greatest effort of many earthquake geologists is invested in detailed mapping of multiple offset markers. Even in the modern age, detailed **tape and compass** recording of fault orientation and horizontal and vertical displacements provide some of the most compelling data available for fault displacements (Figure 7). Field mapping of this type usually includes mapping of linear and point data using mobile differential or real time kinematic (**RTK**) GPS.

All of these approaches may also be used to map and monitor active faults that have not had historical earthquakes on them. One approach that is also commonly used is paleoseismic trenching; whereby shallow excavations are conducted across the surface traces of faults to measure and date subsurface displacements related to both historical and prehistoric earthquakes. The length of surface rupture, and single and multiple event surface displacements, can be compared with global and local earthquake scaling relationships to derive an equivalent magnitude (e.g., Figure 4).

A variety of geophysical methods, including **seismic reflection**, **gravity**, and **aeromagnetic surveys** are also commonly used to investigate active faults in the subsurface. The approach of combining surface and subsurface studies of faults with **analysis of historical seismicity** and **numerical modelling** of fault geometries and displacements (i.e. **rupture models**) is commonly used to characterise earthquake ruptures in high resolution.

## **F. Earthquake frequency-magnitude relationships**

One of the more elegant relationships in earthquake science concerns the relationship between the number of earthquakes and earthquake magnitude, commonly referred to as the **Gutenberg-Richter (G-R) relationship**. Whether one considers a century of global seismicity, or few years of seismicity across an entire continent, or decades of seismicity over a small region, the number of earthquakes equal to or greater than a given magnitude (**N**) increases 10x for every 1.0 increment decrease in earthquake magnitude (typically reported in Richter magnitude,  $M_L$ ). For example, for every  $M_L \geq 5.0$  earthquake, one would expect 10  $M_L \geq 4.0$  earthquakes and 100  $M_L \geq 3.0$  earthquakes. The slope of the best fit line for the logarithm of earthquake populations versus magnitude can be used to calculate a **b value**; typically  $b \approx 1$  for tectonically active regions and ranges from 0.5 to 1.5 across different tectonic environments. The **a value** is a measure of the total seismicity above a given  $M_L$  for a specified region and time.

$$\text{Log}_{10} N = a - b M_L$$

Figure 8 compares G-R relationships for the Canterbury area of New Zealand's South Island for (1) 70 years before (i.e. pre-Canterbury earthquake sequence (CES) seismicity) and (2) 2 years after the 4 September 2010  $M_W$  7.1 Darfield earthquake (CES seismicity). The b values are  $\approx 1$  for the Canterbury seismicity, consistent with expected G-R scaling. The plots show how dramatically the frequency of earthquakes can change for a specified region following a major earthquake (CES seismicity vs pre-CES seismicity), highlighting the role of **aftershocks** and **earthquake clustering** in controlling spatial and temporal distributions of seismicity. Figure 9 shows G-R relationships for different parts of the Australasian region over the same time-scale (100 years), highlighting that the G-R relationship holds well for individual regions even where the frequency of earthquakes is remarkably different.

Although the approximate number of aftershocks following a mainshock may be estimated from the G-R relationship, the rate of aftershocks decays exponentially with time in accordance with the **modified Omori's Law**:

$$n(t) = \frac{k}{(c + t)^p}$$

where  $n(t)$  is the number of earthquakes for a given time (rate),  $k$  and  $c$  are characteristic times,  $t$  is the time after the mainshock, and  $p$  is a constant that modifies the aftershock decay rate. According to this equation, the rate of aftershocks decreases rapidly with time. The rate of aftershocks is proportional to the inverse of time since the mainshock and this relationship can be used to estimate the probability of future aftershock occurrence. Examples of Omori's Law behaviour during the CES are shown in Figure 8b. **P values** typically range from 0.7 to 1.5, consistent with these data. Importantly, a large enough earthquake during an aftershock sequence can reset the aftershock clock and trigger its own aftershock sequence. This is evident after the largest (e.g.,  $M_W \geq 5.9$ ) aftershocks during the CES.

Another feature of aftershock sequences is **Båth's Law**, which states that the difference in magnitude between the **mainshock** and largest aftershock ( $\Delta m$ ) in a sequence is, on average,  $\approx 1.2$ , irrespective of mainshock magnitude. Although Båth's Law is useful for generally considering the magnitude of the largest aftershock, there are numerous instances where (1) the earthquakes initiating a sequence (**foreshocks**) are smaller in magnitude than successive events (e.g., mainshock), (2)  $\Delta m$  is  $\ll 1.2$ , or even 0 (termed **earthquake doublets**), or (3)  $\Delta m$  is  $> 1.2$ . Caution must always be

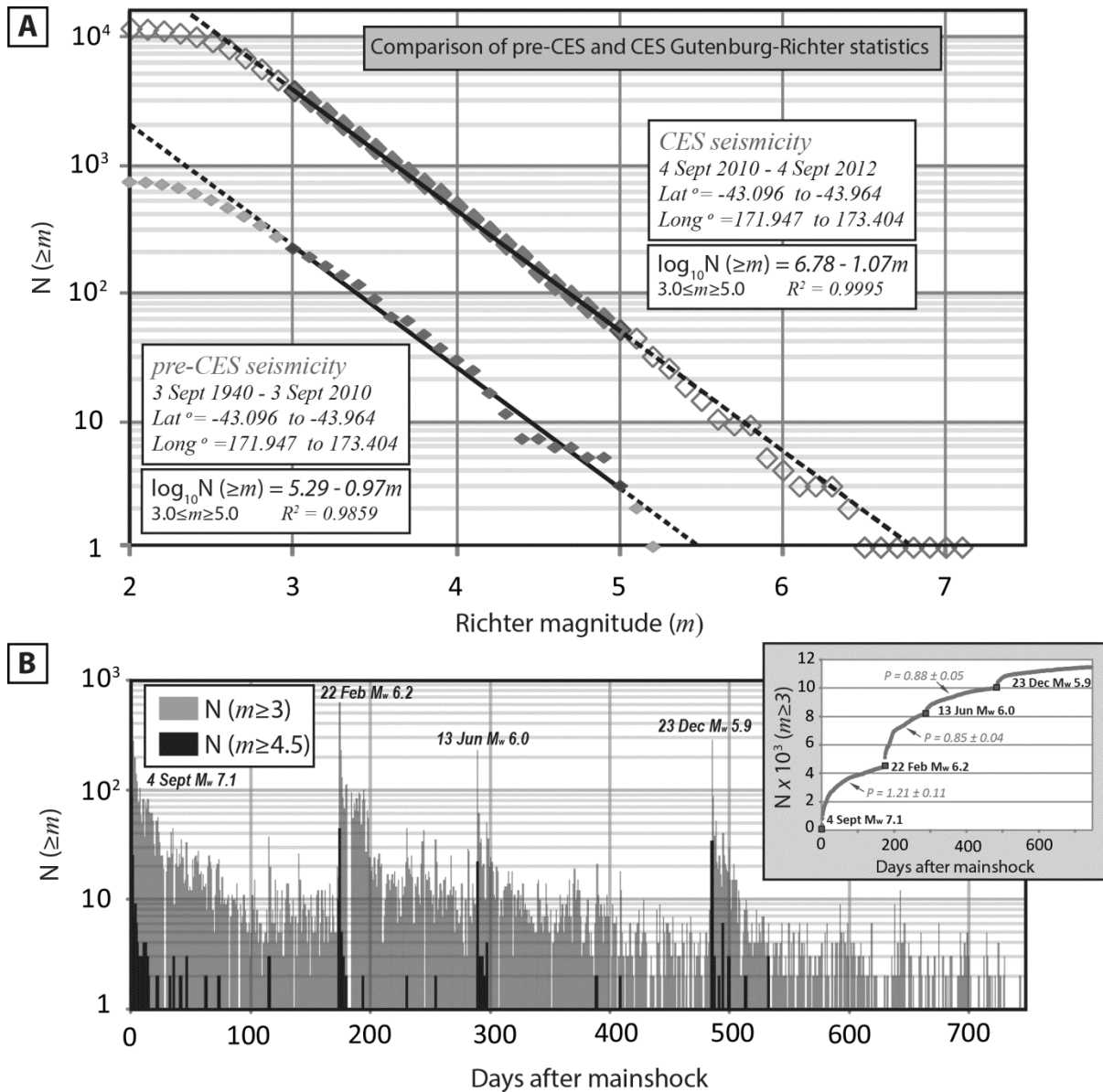


**Figure 8.** A) Gutenberg-Richter plot for frequency-magnitude relationships in the Canterbury region (see lat-long values for spatial extent) in the 70 years prior and two years after the Darfield earthquake. B-values ( $\sim 1$ ) are determined for Richter magnitudes between 3.0 and 5.0 and subject to curve fitting uncertainties of  $\sim 10\%$ ; both datasets adhere well to G-R relationship ( $R^2$  as shown). Catalogue completeness issues are not addressed in this study. Post Darfield annual seismicity rates between  $M_L$  3 to 5 increase from pre-CES rates by an average of  $4.2 \times 10^4 \%$ .

(B) Temporal distribution of  $M_L \geq 3.0$  and  $M_L \geq 4.5$  earthquakes during the Canterbury earthquake in days after the Darfield earthquake (4:35 am NZ standard time) binned into 24 hr increments. Changes in seismicity rate reflect timing of larger (i.e.  $M_w \geq 5.9$ ) earthquakes, in accordance with Omori's Law.

(B Inset) shows cumulative total of  $M_L \geq 3.0$  earthquakes with time, showing punctuated rate changes immediately preceding the four largest CES earthquakes, in accordance with Omori's Law. P-values describing seismicity decay rate exponent are from Shcherbakov et al. (2012). All seismic data from [www.geonet.org.nz](http://www.geonet.org.nz)

applied when using Båth's Law to forecast the likely maximum magnitude of future earthquakes; in the case of the  $M_L$  7.1 Darfield earthquake, the largest aftershock on 13 June 2011 was  $M_L$  6.4 ( $\Delta m \approx 0.7$ ) (Figure 8).

## **G. Earthquake hazards**

Earthquake hazards can be generally classified as either **faulting-induced** or **shaking-induced**. Faulting-induced hazards are those directly attributable to displacements across a fault or fault zone. Shaking-induced hazards are those attributable to earthquake-induced strong ground motions. A summary of faulting and shaking induced hazards is shown in Figure 10.

### *G.1. Faulting-induced hazards*

Faulting-induced hazards can be caused by faults that rupture through to the surface or terminate in the subsurface. For faults that break the surface, **deformation and/or fracturing of lifelines** (e.g., roads, power lines, bridges, internet cables, pipelines, sewers), **buildings** (e.g., houses, power stations), and other infrastructure (e.g., fences, irrigation channels) are an obvious hazard ('1' in Figure 10). The distance between features such as power poles may be increased or decreased depending on their orientation with respect to the fault and the type of displacement; in extended areas power lines may be snapped and in contracted areas they may go slack. **Fault rupture of gas lines** could induce fires if ignition sources exist. **Fault rupture through dams** ('2' in Figure 10) can result in partial or complete dam collapse and subsequent flooding. **Changes in relative land elevations** across fault scarps can affect rivers in several ways; inducing **ponding and flooding** ('3a' in Figure 10), **channel migration or avulsion** (i.e., occupation of new stream channels and abandonment of previous stream channels; '3b' in Figure 10), the creation of **waterfalls** (i.e., knickpoints) or other changes in stream gradients, and **changing stream discharge** along the channel (e.g., reducing discharge, '3c' in Figure 10). Surface fissures pose obvious hazards in both urban and rural environments, for example, humans and animals may be at risk of injury from **falling into fissures** ('4' in Figure 10). Fault surface ruptures can cause **major damage to forests**, including tree fall ('5' in Figure 10). Surface ruptures can also **affect the behaviour of mass movement hazards** such as landslides and rockfalls. Surface ruptures underneath the ocean can induce **tsunamis** and mass movements such as **turbidites**. Faults that terminate within the subsurface may **rupture or deform buried infrastructure** (e.g. tunnels; '6' in Figure 10) and other deep anthropogenic features such as **mines** and **nuclear waste repositories**. Subsurface faulting **can affect the geometry and dynamics of hydrologic and geothermal systems** and thus influence industries that extract water, oil, gas, and other fluids and gases from the subsurface ('7' in Figure 10).

In coastal environments, faulting may cause **uplift or subsidence** and thus affect flood and marine inundation hazards. Rapid submergence of terrestrial environments or emergence of submarine environments has been documented in several instances. Elastic strain in the interseismic period and post-seismic deformation (Figure 4) may also influence the fault hazards described above.

The propagation of a fault rupture through to the surface or shallow subsurface depends upon the hypocentre of the earthquake, the rupture size and geometry, and the amount and direction of slip on the fault. For shallow (e.g. crustal) earthquakes, the minimum earthquake  $M_W$  (i.e. **seismologic threshold**) to induce surface rupturing ranges widely, from  $M_W$  5 to 6.9. Deeper earthquakes,

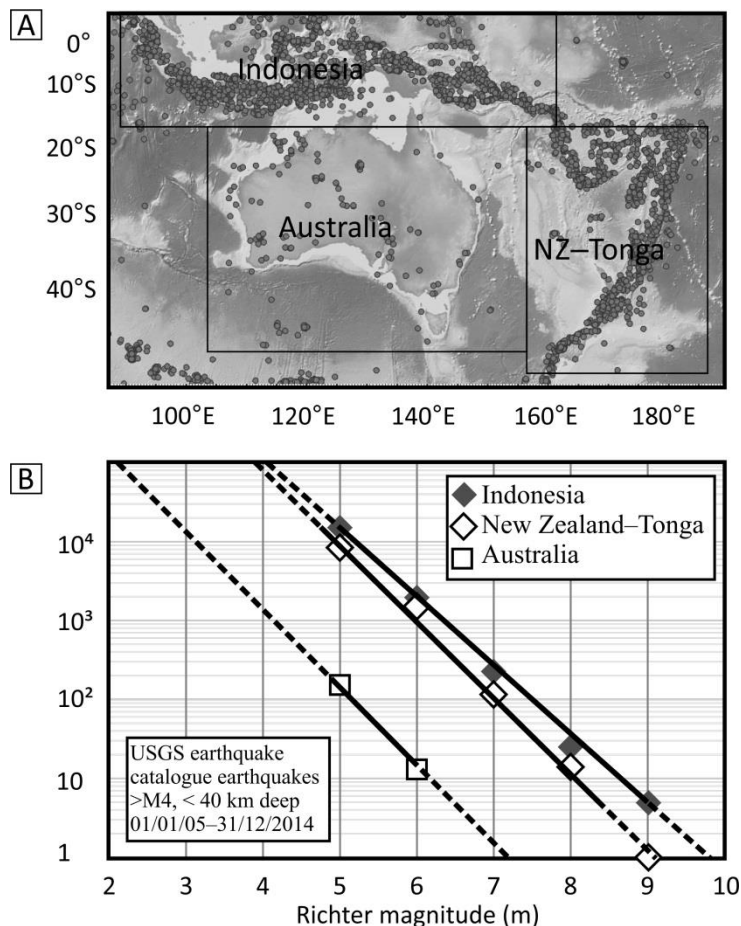


**Figure 9.** A) Epicentral locations of  $M_w \geq 5$  earthquakes in Australasia since 1905. Boxes correspond to boundaries of different regions shown in (B).

(B) Gutenberg-Richter plot summarizing  $M_w \geq 5$  seismicity for the regions delineated in (A) for time period spanning 1905 to 2014.

including those associated with subduction zones, may be quite large ( $M_w \geq 7.8$ ) without causing surface rupture on the land or seafloor.

### G.2. Shaking-induced hazards

The passage of seismic waves through natural and built environments causes shaking at a variety of amplitudes, durations, and frequencies. Shaking of sufficient intensity, duration, and/or frequency may initiate a variety of earthquake induced processes. The characteristics of shaking required to induce these processes may be referred to as a **seismologic threshold**. Seismologic thresholds may be defined by PGAs, PGVs, or PGDs, earthquake magnitudes, shaking durations above certain intensities, shaking intensities at certain frequencies, and/or metrics that combine some or all of the above. It is important to remember that all of the shaking-induced hazards we describe below may also occur in the absence of seismic shaking, or in earthquakes below seismologic thresholds.

In areas of sufficient steepness and relief, earthquakes can trigger **mass movements** of soil and rock including **rockfalls** and **boulder rolls** ('8' in Figure 10), **landslides** in both terrestrial and subaqueous environments ('9' in Figure 10), **cliff collapses** and **rockslides** ('10' in Figure 10), and a variety of other phenomena including **soil lateral spreads**, **slides**, **slumps**, **earth flows** and **avalanches**, and **rock avalanches**, **boulder displacements**, and **bedrock fracturing** including **sackungen**. In caves,

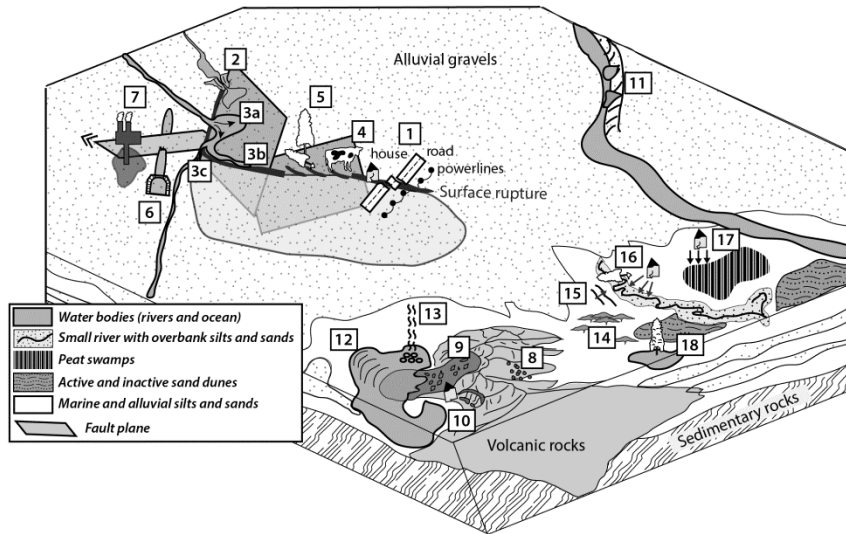


**Figure 10.** Earthquake faulting and shaking hazards in a geologically heterogeneous landscape. See Section D for detailed descriptions of the pictured phenomenon. Faulting-induced hazards include deformation and/or fracturing of structures and lifelines (1) including fault rupture through dams (2), changes in land elevation and subsequent ponding and flooding (3a), channel migration or avulsion (3b), and/or changes in stream discharge (3c), ground fissuring and risk to humans and animals (4), damage to trees (5), rupture or deformation of buried infrastructure by blind faults (6), and alteration of the geometry and dynamics of hydrologic and geothermal systems (7). Shaking hazards include rockfalls and boulder rolls (8) landslides in both terrestrial and subaqueous environments (9), cliff collapses and rockslides (10), landslides into rivers (11), landslide-induced tsunamis (12), changes in spring temperature, chemistry, and/or discharge (13), liquefaction (14), lateral spreading (15), ground failure induced damage to surface and subsurface structures and lifelines (16), surface subsidence (17), and submergence of natural and built environments near water bodies (18).

strong shaking may cause damage to speleothems and cave collapses. Where mass movements interact with marine or terrestrial water bodies, they may influence the morphology and dynamics of rivers ('11' in Figure 10) including formation of lakes upstream of landslides and changes to the amount and type of material entering streams, and may cause perturbations such as tsunamis ('12' in Figure 10). Earthquake shaking and associated rock fracturing and fluid mobility can induce changes in the **temperature or discharge of springs**, or form **new springs** ('13' in Figure 10). Shaking may transform granular materials from a solid to liquefied state (i.e. **liquefaction**) as a consequence of increased pore-water pressure, resulting in formation of **sand blows** where liquefied materials are ejected to the surface ('14' in Figure 10) and **lateral spreading fissures** where materials overlying the liquefied layer are displaced laterally ('15' in Figure 10). Lateral spreading may cause changes in river morphology, and may cause damage to natural and built environments such as **tree toppling, house and building damage, and damage to surface** (e.g. bridges and roads) and **buried** (e.g. sewers, power cables) **lifelines** ('16' in Figure 10). Liquefaction is also typically accompanied by **surface subsidence** ('17' in Figure 10) which can cause submergence of natural and built environments near water bodies ('18' in Figure 10). Strong shaking and related liquefaction-induced surface deformations and subsidence in coastal environments may **influence flood and marine inundation hazards** long after the earthquake sequence has finished (Hughes et al. 2014), highlighting the concept of **cascading hazards**, whereby initial (coseismic) hazards influence subsequent (post-

seismic) hazards. Another example of a cascading hazard is a mass movement on to a glacier, which can reduce glacial ablation and cause the toe of the glacier to extend.

Typical **seismologic thresholds for mass movements** are approximately earthquakes  $\geq M_w$  4 to 6.5, MMIs  $\geq$  V to VII, PGAs  $\geq$  0.2-0.4 g, and PGVs  $\geq$  12-25  $\text{cm s}^{-1}$  (depending on type of mass movement, source location and characteristics, and site characteristics). Typical **seismologic thresholds for liquefaction, lateral spreading and subsidence** are approximately earthquakes  $\geq M_w$  5, MMIs  $\geq$  VII, PGA  $\geq$  0.2 g, and magnitude-weighted PGAs (i.e. PGAs corrected for shaking duration) of  $\geq$  0.1 g. In general, the density and severity of a given phenomenon at a specified site scales with the intensity of shaking, while the spatial distribution of the phenomena over a region scales with the magnitude of the earthquake, which influences the spatial distribution of shaking.

### *G.3. Assessing, avoiding, and mitigating earthquake hazards*

Most faulting-induced hazards arise due to displacement at the ground surface, so understanding the nature and magnitude of that displacement, and its relation to other landscape elements such as slopes and streams, is critical for development of resilient near-fault communities. In general, the larger the infrastructure, the more important it is to conduct a rigorous seismic hazard analysis. Fault hazard mitigation at a late stage in a project can be costly in terms of both time and money as occurred with the Clyde Dam in Central Otago, New Zealand, where a slip joint had to be installed to allow up to 2m of movement on the Clutha River fault, which passes through the dam foundations (Hatton et al., 1987).

A variety of techniques exist for assessing, avoiding, and mitigating fault rupture and earthquake shaking hazards. These are described in detail in the Supplementary Information section accompanying this chapter.

## **H. Case study: The 2010 to 2011 Canterbury earthquake sequence in New Zealand's South Island**

### *H.1. Seismology*

The Canterbury earthquake sequence (CES) began with the 4 September 2010  $M_w$  7.1 Darfield earthquake (Figures 8, 11). This mainshock triggered an aftershock sequence including four earthquakes of  $M_L \geq 5.9$  and more than 4000 earthquakes of  $M_L \geq 3$  (seismic data obtainable from [www.geonet.org.nz](http://www.geonet.org.nz)). The most damaging aftershock was the 22 February 2011  $M_w$  6.2 Christchurch earthquake, which caused 185 fatalities and US\$ 15 to 20 Billion damage to buildings and infrastructure. Large damaging aftershocks also occurred in June and December 2011. The CES exhibited well-defined Gutenberg-Richter frequency-magnitude scaling (Figure 8a) and modified Omori's Law behaviour following major events (Figure 8b) (Shcherbakov et al., 2012).

The epicentre of the Darfield earthquake was approximately 44 km west of the Christchurch, with a hypocentral depth of  $\sim$  11 km (Figure 11) (Gledhill et al., 2011). Local and regional seismometers indicated initial reverse motion at the hypocentre however CMT solutions reveal that most of the seismic energy was associated with dextral strike-slip faulting (Figure 11). The epicentres of the 22 Feb and 13 June Christchurch earthquakes were to the south of the city, within 5 km of the Central Business District. Both of these earthquakes involved complex ruptures on 2 or more faults (Figure 11) (Beavan et al., 2012). The epicentre of the 23 December earthquake was offshore, approximately 5 km northeast of the CBD. The focal mechanisms for these earthquakes are shown in Figure 11.

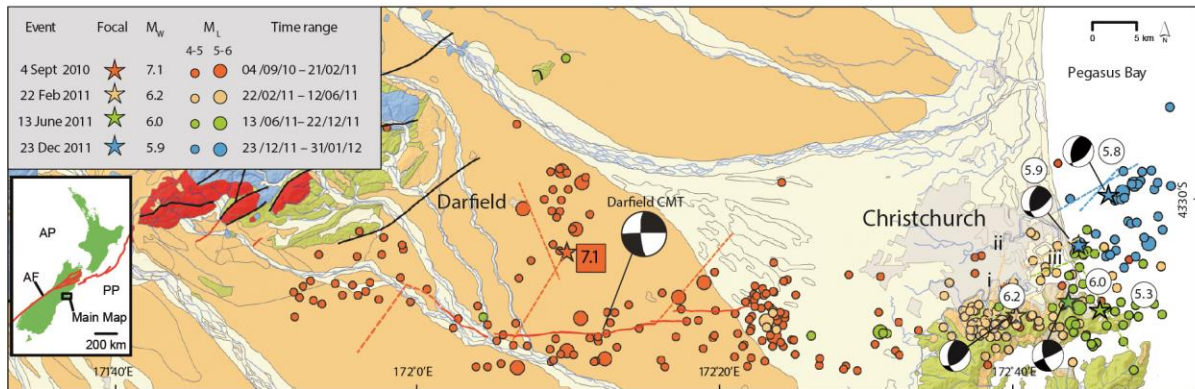


**Figure 11.** The geologic and seismologic context for the 2010-2011 Canterbury earthquake sequence. Inset shows location of main map in New Zealand's South Island, AF=Alpine Fault, PP = Pacific Plate, AP = Australia Plate. On main map, dashed lines are surface projections of tops of blind faults, solid line is surface rupture trace along the Greendale Fault. The Heathcote (i) and Avon Rivers (ii) drain into the Avon-Heathcote Estuary (iii). Earthquake epicentres for events of  $M_L \geq 4$  coded for magnitude grouping by size and by colour coding for time. Stars denote epicentral locations for largest earthquakes in the sequence. Focal mechanisms for largest events as shown. Lithologic descriptions as follows: Blue = Mesozoic sedimentary rocks, Red = Tertiary sedimentary rocks, Green = Tertiary volcanic rocks, Yellow = Pleistocene sediments, Light Grey = Holocene sediments.

Most earthquakes had hypocentres within greywacke rocks that comprise most of the brittle crust in the Canterbury region.

The proximity of the large aftershocks to Christchurch caused strong intensity shaking throughout the city (Bradley et al., 2014). PGAs > 1 g were locally recorded in parts of Christchurch, with PGAs > 0.4-0.8 g in the CBD, during the Feb and June earthquakes. Amplification of strong ground motions relative to bedrock motions was a common characteristic of many CES earthquakes; strong topographic amplification occurred in hill suburbs south of the city, strong amplification occurred throughout the eastern parts of the city due to liquefaction effects, and strong amplification occurred in valleys fringing the southern part of the city due to basin edge effects.

The annual frequency of earthquakes during the CES was 500-550 times higher than the annual frequency of earthquakes of equivalent magnitudes averaged over the preceding 70 years. It was known that the Canterbury region was experiencing NNW-SSE oriented tectonic shortening at roughly  $2 \text{ mm yr}^{-1}$  (Wallace et al., 2007) and that active faults were likely to lurk undiscovered throughout the region (Pettinga et al., 2001). However, none of the faults responsible for the Darfield earthquake or large CES aftershocks were known prior to the CES.

## H.2. Fault rupture and surface displacements

Seismologic and geodetic studies helped to define the location, geometry, and slip distributions of the faults responsible for the CES (e.g. Elliot et al., 2012; Beavan et al., 2012). The Darfield earthquake involved the complex rupture of at least 6 faults with different orientations, kinematics, and slip distributions (Beavan et al., 2012). The rupture of all of the faults probably took around 40-45 seconds. The Greendale Fault rupture likely involved  $\sim 3 \text{ km/s}$  rupture velocities (Holden et al., 2011) with strong directivity towards Christchurch. The only fault to produce a surface rupture was the Greendale Fault. The surface rupture was approximately 30 km long surface rupture (Quigley et al., 2012). The surface rupture morphology and associated coseismic displacements were extensively studied using field, lidar, InSAR, and geodetic techniques (Figure 12). The Greendale Fault rupture

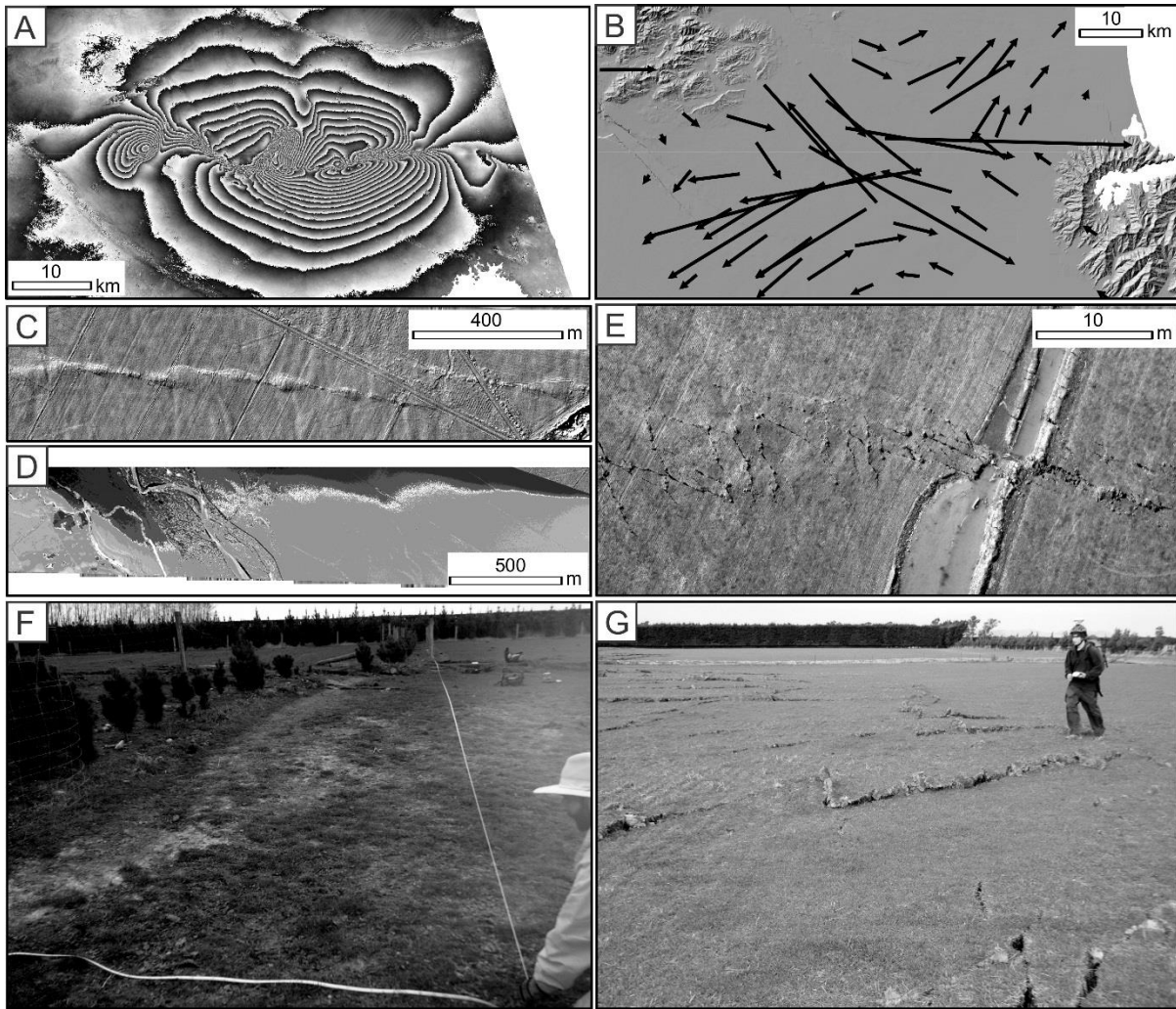


**Figure 12.** Recording of the Darfield earthquake surface rupture: (A) D-InSAR; (B) Geodetic GPS; (C) LiDAR; (D) Differential LiDAR; (E) Aerial photography; (F) Tape and compass field measurements; (G) RTK/differential GPS field measurements.

produced mainly right-lateral displacements across flat, grassed farmland (Quigley et al., 2010a, 2010b; Barrell et al., 2011). The intensive agricultural land-use of the Canterbury Plains provided over 100 displaced cultural markers that could be measured with high precision (e.g., roads, fences, crop rows, plough-lines, canals, tree-lines and power-lines). The surface rupture had a maximum right-lateral surface displacement of 5.3 m and average displacement of ~2.5 meters (Quigley et al., 2012). Maximum subsurface slip on the Greendale Fault occurred at depths of 2 to 6 km (Beavan et al., 2012) and may have exceeded 7 m over a strike length of ~7-8 km (Elliott et al., 2012). Surface displacements above areas of maximum inferred subsurface slip typically range from 4-5 m, indicating a gradual (~1m per km) vertical decrease in coseismic slip towards the ground surface. The Greendale Fault has been interpreted as a Cretaceous normal fault that was subsequently reactivated as a strike-slip fault in the modern tectonic regime. The last major earthquake on this fault, prior to the Darfield earthquake, was dated to ca. 20-30 kyr ago (Hornblow et al., 2014).

The 22 February 2011  $M_w$  6.2 Christchurch earthquake involved the rupture of 2 or 3 blind faults (Figure 11) with reverse and right-lateral displacements (Beavan et al. 2012). The rupture was inferred to reach as shallow as ~0.5 km depth below the surface, suggesting rupture termination in

Miocene volcanic rocks. Maximum coseismic slip was 2.5 to 3 m at depths of 4–6 km (Beavan et al. 2012). Constraints on surface deformation above the fault ruptures are provided by continuous GPS (cGPS), geodetic campaign GPS, differential InSAR, and differential LiDAR. Differential InSAR, differential LiDAR, and cGPS were used to determine land elevation displacements resulting from faulting and shaking-induced subsidence, liquefaction, and lateral spreading (Beavan et al., 2011; Hughes et al., 2014).

The 13 June 2011  $M_w$  6.0 earthquake likely involved an intersecting ENE-striking reverse-right lateral fault and NW-striking left-lateral fault with the shallowest rupture extent at  $\sim 1$  km depth and maximum subsurface slip of  $<1$  m (Figure 11) (Beavan et al. 2012). The 23 December 2011  $M_w$  5.8 and 5.9 earthquakes ruptured 1–2 largely offshore, NE-striking reverse-right-lateral, blind faults with maximum slip of  $>1.4$  m occurring at depths of 2–5 km and shallowest rupture extents of  $\sim 1$  km depth (Figure 11) (Beavan et al. 2012). Details of the evolution of the CES seismicity are summarized in detail in Bannister and Gledhill (2011).

### *H.3 Fault rupture hazards*

About a dozen buildings, mainly single-storey houses and farm sheds, were affected by the Greendale Fault surface rupture, but none collapsed, largely because most of the buildings were relatively flexible and resilient timber-framed structures and also because deformation was distributed over a relatively wide zone (Van Dissen et al., 2011, 2013). In one case, a discrete fault with  $\sim 0.5$  metres displacement passed right through the front door of a single story modern brick-clad house, causing major irreparable structural damage, however the residents continued to occupy the house for weeks after the earthquake. The fault passed beneath a power substation; however no major structural damage occurred. Roads, train tracks, power lines, underground pipes, fences, and irrigation channels were also deformed by surface fault rupture and suffered damage commensurate with the type of feature, its orientation to the fault, and the amount, sense and width of surface rupture deformation. In some cases roads suffered major fissures and had to be repaved over distances exceeding 100 metres. Many fences had to be repaired. Property boundaries changed shape, requiring re-surveying. Poplar, eucalypt and/or pine trees close to the fault trace shelter belts were commonly damaged, and some trees subsequently toppled. Open fissures across agricultural areas required cultivation and filling to reduce the risk of damage to livestock and irrigation and farming equipment (Almond et al., 2010). Differential vertical motion across the fault scarp caused partial avulsion of the Hororata River, which led to extensive flooding throughout the agricultural area (Duffy et al., 2013).

Although the largest CES aftershocks did not cause surface rupture, they caused surface folding that subsequently influenced flood and marine inundation hazard in Christchurch by changing the elevation of the land surface (Hughes et al., 2015). The Avon River (Figure 11) was affected by cumulative tectonic subsidence throughout its reach, until it crosses the up-dip surface projection of one of the 22 Feb 2011 fault ruptures. The tectonic influence on the Avon River lowered the channel with respect to sea-level, and thus increased the potential for flooding along the river. The Heathcote River (Figure 11) tectonically subsided in its upstream reach and tectonically uplifted in its downstream reach, with a change across the up-dip surface projection of another one of the 22 Feb 2011 fault ruptures. The tectonically-induced reduction in river gradient associated with downstream uplift is expected to increase flooding in the upstream reach by reducing stream power

across the fault. The Avon-Heathcote Estuary (Figure 11) experienced cumulative tectonic uplift throughout its spatial extent. This uplift is expected to increase flooding in both the Avon and Heathcote Rivers due to a reduction in stream power.

#### *H.4 Earthquake shaking hazards*

Many of the largest CES earthquakes caused liquefaction in Christchurch and the surrounding region. The most severe liquefaction events in Christchurch occurred during the 2010 Darfield mainshock and the largest aftershocks in February, June, and December 2011 (Quigley et al., 2013).

Liquefaction surface features included sand blows, fissures, and lateral spreads. In highly susceptible areas, the thickness and areal extent of sand blows increased with increased magnitude-weighted PGA. Lateral spreading occurred in the earthquakes with highest magnitude-weighted PGAs.

Lateral spreading was typically most severe on the low elevation, inner meander loops of rivers within 30-40 metres of the active river channel. Liquefaction-induced surface subsidence exceeded 40 to 50 cm in some areas. Faulting and shaking-induced changes in land elevations influenced the spatial distribution and health of a variety of flora and fauna. The combination of flood-plain subsidence, lateral spreading (which caused channel narrowing and shallowing), and river channel sedimentation (which caused channel shallowing), together with the tectonic influences described above, collectively increased flood hazard over much of eastern Christchurch (Hughes et al., 2015). The severity of damage to houses, underground lifelines (e.g. sewers, water mains), bridges and road correlated well with the areal extent of liquefaction and the amount of surface subsidence. As a result of severe and recurrent liquefaction damage, and the infeasibility of timely and effective land repair, more than 7000 residential properties in Christchurch were red-zoned and purchased by central government at a cost exceeding NZ \$ 1.6 billion.

Mass wasting phenomena including rockfall, cliff collapse, boulder roll and displacement, landslides, and loess fissuring occurred throughout the Port Hills area of southern Christchurch and in more isolated parts of Banks Peninsula during several CES earthquakes. Cliff collapses on lower slopes destroyed buildings both above and below the cliffs. Collapses on higher slopes released thousands of rockfalls. The most severe rockfall event (~6000 boulders) occurred during the 22 Feb Christchurch earthquake, when rockfalls damaged about 200 homes and caused 5 fatalities. Rockfalls were observed over an area of ~65 km<sup>2</sup> in the Feb 22 Christchurch I earthquake and ~40 km<sup>2</sup> in the largest June earthquake. Boulder volumes ranged from < 1 m<sup>3</sup> to > 15 m<sup>3</sup>. Boulder run-out distances locally exceeded 700 metres from the source cliff. Some sites in the Port Hills experienced ≥ 5 separate rockfall events, including the Darfield earthquake (Mackey and Quigley, 2014; Massey et al., 2014). The PGA (horizontal) threshold for rockfall triggering was estimated at 0.3 to 0.4 g (Massey et al., 2014). Mackey and Quigley (2014) derived a threshold PGV of 12 ± 1 cm/s for the localized detachment of susceptible rocks in a previously fractured rock mass, 17 ± 2 cm/s for localized rock fracture and rockfall in an intact rock mass, and 25–30 cm/s for extensive rockfall and rock mass fracturing (such as that which was observed in the February earthquake). Importantly, the occurrence of rockfall during earthquakes did not reduce the risk of future rockfall from the source areas; although many susceptible rocks were removed, extensive rock mass fracturing during earthquakes increased the susceptibility to rock mass failure in future earthquakes by creating additional loose material. More than 700 residential properties were red zoned in the Port Hills on the justification that estimated individual annual fatality risk values exceeded societally acceptable

values. Landsliding also occurred in the Harper Hills on the western edge of the Canterbury Plains (Stahl et al., 2013) and on gravel cliffs flanking the Rakaia River in the Darfield earthquake. The Harper Hills landslide generated a discontinuous headscarp exceeding 2.5 km in length with ~30-40 cm of extensional movement across the fissure. A PGA  $\approx$ 0.45 g was estimated to have triggered this landslide (Stahl et al., 2013).

The CES generated widespread hydrological effects ranging from coseismic changes of groundwater levels in boreholes, to more sustained (days to weeks) post-seismic changes in spring flow, river discharge and groundwater piezometric levels, to longer term shifts ( $> 1$  yr) in groundwater level (Cox et al., 2012). Large increases in local groundwater levels ( $>20$  m) were observed around the Greendale Fault. Wells in coastal confined aquifers in Christchurch showed jumps of  $> 1$  m that persisted for  $\geq 8$  days (Gulley et al., 2013). Groundwater levels and springs were affected throughout New Zealand at distances up to almost 1000 km away (Cox et al., 2012), including temperature and geochemical changes in springs proximal to the plate boundary Alpine Fault (Cox et al., 2014) at a distance of  $\sim$ 180 km from the Darfield earthquake. Shaking intensities at distal areas of hydrologic response were low (e.g. PGA  $<0.005$  g), highlighting the ability of large earthquakes to induce changes in rock permeability at great distances.

#### *H.5. Assessing, avoiding, and mitigating future earthquake hazards in Christchurch*

Following the Darfield earthquake, surface and subsurface investigations of the Greendale Fault were conducted to determine the frequency of fault surface ruptures and develop criteria for fault set-back distances. A fault avoidance zone was defined (Villamor et al., 2012) based on detailed maps of surface fissures and displacements (Van Dissen et al., 2011, 2013). The fault is assigned to Recurrence Class VII (Kerr et al., 2003), meaning that the only designated building restrictions are to critical post-disaster facilities (all other infrastructure types are permitted). Some residents had their houses rebuilt within metres of the sites of their old, damaged houses.

Seismic hazard mitigation in Christchurch has been improved through a mixture of changes to the building code and rezoning of residential land. For small structures, the seismic component to building codes was increased by 36% in Christchurch following the 22 Feb earthquake, although larger projects generally require site-specific investigations. A review of residential areas following the earthquake established a residential red-zone, which encompasses all land within which land repair is presently uneconomic (see Supplementary Information). This zone is primarily based on liquefaction resistance, as derived from extensive post-earthquake CPT surveys. However, it also accounts for the increased flood hazard to land that has subsided. Beginning after the June Christchurch earthquake, the Christchurch City Council began to construct gravel levees around the Avon River to elevations equivalent to the pre-Darfield earthquake floodplain elevation. Tide-induced flooding by raising of the water table to the ground surface is common in the red-zone outside the levees, and parks located with them flood regularly. Mitigation of liquefaction hazards involved soil remediation methods to reduce the deformability of the ground and inhibit the development of high pore water pressures. Favoured techniques included densification of the ground by compaction methods; solidification by grouting and techniques that hasten cementation; prevention of lateral movements using containment structures; drainage of pore pressures by increasing permeability through the use of stone columns or drains. Where sites are difficult or

expensive to remediate, differential settlement can be reduced by construction of foundations that have sufficient capacity to resist both earthquake shaking and differential movements.

Bastin et al. (2015) identified paleo-liquefaction in parts of eastern Christchurch and attributed these to the 1869  $M_w$  4.9 Christchurch (Addington) earthquake and / or preceding prehistoric events in the last ca. 500 yrs. Bastin et al (2013) mapped thousands of lateral spreading cracks and concluded that properties within 40 meters of the Avon River were the most severely affected, implying that the enforcement of setback distances of this amount in highly liquefiable areas could help reduce liquefaction damage. Quigley et al. (2013) showed that liquefaction feeder dikes were repeatedly reactivated throughout the CES, implying that the distribution of past liquefaction provides important constraints on the locations of future liquefaction.

A variety of retaining walls existed throughout Christchurch, and performed to varying levels. In general, engineered walls performed better than non-engineered walls, even when they had not been designed with seismic loadings in mind. Several failures were attributable to up and/or down-slope instabilities that overloaded/undermined the walls, indicating the need for a comprehensive site model that extends beyond the site footprint. Walls that retained undisturbed, dry loess performed better than those that retained fill. Outward movement was common, even for well-engineered walls, and was particularly notable for flexible constructions like gabion walls.

GIS analysis of rockfall distribution relative to topography and urbanisation was used to develop a life-safety risk assessment for the entire Port Hills area (Heron et al., 2014). A systematic study incorporating future rockfall probabilities, probabilities of persons being in the path of rockfalls, probabilities of persons being present at a specific location, and probabilities of persons being killed if struck by rockfalls were used to estimate the annual individual fatality risk from rockfall in the Port Hills and aid in Red Zone delineation (Massey et al., 2014). Mackey and Quigley (2014) dated the penultimate severe rockfall at one location in the Port Hills to ca. 6-8 kyr ago, and argued that this provided a preliminary constraint on the return time of strong PGVs analogous to those encountered in the February and June earthquakes. Scaling of loose boulders and stabilizing susceptible rock masses could reduce the risk of future rockfall fatalities.

## **I. SUMMARY**

- Earthquakes occur on active faults in all tectonic settings, including intraplate settings. The damage and collapse of engineered structures during strong earthquake shaking is responsible for the largest number of earthquake fatalities on average however in some locations, tsunamis or landslides pose the biggest risk to life and infrastructure. Seismic risk is characterised by the combination of seismic hazard, exposure to earthquakes, and the vulnerability of humans and infrastructure to the effects of earthquakes. Seismic hazard, exposure, vulnerability, and risk vary widely throughout the Australasian region due to tectonic setting, geology, and societal factors.
- Active faults are typically characterised by their length and width, which control the rupture area and  $M_w$  potential. Other important parameters when considering the hazard posed by active faults are the earthquake recurrence interval and fault slip rates. Active faults may be exposed at the surface as fault scarps, or buried by surface processes, or blind. The earthquake recurrence interval generalized by the concept of a

seismic cycle comprising interseismic, coseismic, and postseismic periods. The seismic cycle appears to be somewhat periodic for some faults and highly irregular for others.

- Earthquakes may be triggered by a multitude of surface and subsurface processes that influence the stress field, geologic conditions, and hydrologic conditions in and around the fault. Human activity can induce earthquakes however earthquakes are a natural process that has been active for billions of years, long before humans inhabited the planet.
- Earthquakes can be measured using a variety of aerial and surface measurement techniques, seismology, geophysics, and other approaches. Many of these data sets are important towards documenting how earthquakes have affected the natural and built environments, with the goal of avoiding or mitigating the effects of future earthquakes through active fault zoning, land rezoning or remediation, refining earthquake building codes, and other approaches.
- Earthquake shaking is typically characterised in terms of intensity measures (peak ground displacement, velocity, and acceleration), duration, and frequency content. These parameters can be strongly influenced by the characteristics of the earthquake rupture (source effects such as  $M_w$  and directivity), path effects (influenced by lithospheric composition and structure) and site effects (influenced by topography, geology, etc). Stronger intensity shaking can be produced at a given site by smaller  $M_w$  but more proximal earthquakes; this was the case for the more damaging 2011  $M_w$  6.2 February earthquake in Christchurch compared to the preceding 2010  $M_w$  7.1 Darfield earthquake. The distribution and severity of shaking hazards such as rockfall, landslides, liquefaction, lateral spreading, and subsidence relate to the characteristics of earthquake shaking. Land planning strategies can be used to avoid these hazards, and engineering strategies can be used to mitigate their impacts.

## **J. REVIEW QUESTIONS**

1. Draw a sketch of a hypothetical fault undergoing unilateral rupture propagation, showing the following (a) hypocentre, (b) epicentre, (c) centroid, (d) surface rupture, (e) subsurface rupture length and width, (f) rupture propagation direction, (g) area of strongest expected shaking due to directivity effects.
2. What are the methods that could be used to document surface deformation immediately following an earthquake with a surface rupture?
3. Using the rupture areas provided in Figure 4, create your own list of landmarks or other features with areas roughly equivalent to  $M_w$  3 to 9 earthquake ruptures.
4. How would you expect the following characteristics to vary for an equivalent  $M_w$  intraplate earthquake versus a plate boundary fault earthquake (a) crustal attenuation and felt distances, (b) stress drop, (c) fault recurrence interval?
5. Write a list of earthquake hazards in natural and built environments induced by (a) fault rupture, and (b) shaking.

### **K. DISCUSSION QUESTIONS (5)**

1. What controls whether a fault (a) ruptures the surface and remains preserved as a fault scarp, or (b) ruptures the surface but is subsequently buried, or (c) does not rupture the surface (e.g. blind rupture). Discuss how earthquake recurrence interval may contribute to (a) vs (b).
2. Discuss how different earthquake triggering mechanisms might affect the recurrence interval of earthquakes on a given fault.
3. How could the Gutenberg-Richter relationship and Bath's law be used to discuss the likely magnitudes of earthquakes in an aftershock sequence following a mainshock?
4. What are the three most important characteristics of earthquake shaking and how might these characteristics be affected by source effects and site effects?
5. Discuss what you think are some of the key lessons to learn from the 2010-2011 Canterbury earthquake sequence in New Zealand.

## **FURTHER READING AND REFERENCES CITED**

Ambraseys, N., & Bilham, R. (2011). Corruption kills. *Nature*, 469(7329), 153-155.

Allen, J., and 19 others including Quigley, M., (2014) Geotechnical & Flooding Reconnaissance of the 2014 March Flood Event Post 2010-2011 Canterbury Earthquake Sequence, New Zealand, GEER Report, 134 p.

Almond, A., Wilson, T. M., Shanhun, F., Whitman, Z., Eger, A., Moot, D., Cockcroft, M., Nobes, D. C. (2010). Agricultural land rehabilitation following the 2010 Darfield (Canterbury) Earthquake: a preliminary report. *Bulletin of the New Zealand Society for Earthquake Engineering*, 43(4), 432.

Andrus, RD & Stokoe, KH 2000, 'Liquefaction resistance of soils from shear-wave velocity', *Journal of Geotechnical and Geoenvironmental Engineering*, vol. 126, no. 11, pp. 1015-25.

Bannister, S.C.; Gledhill, K.R. 2012 Evolution of the 2010-2012 Canterbury earthquake sequence. *New Zealand Journal of Geology and Geophysics*, 55(3): 295-304; doi: 10.1080/00288306.2012.680475

Bastin, S., Quigley, M., Bassett, K., (2013) Modern and paleo-liquefaction features in eastern Christchurch and strategies for locating pre-historic liquefaction, Proc. 19th NZGS Geotechnical Symposium, 8 p.

Bastin, S., Quigley, M., and Bassett, K., (2015) Paleoliquefaction in eastern Christchurch, New Zealand, *GSA Bulletin*, accepted

Barrell, D., N.J. Litchfield, D.B. Townsend, M. Quigley, and 20 others, 2011, Strike-slip ground-surface rupture (Greendale Fault) associated with the 4th September 2010 Darfield Earthquake, Canterbury, New Zealand, *Quarterly Journal of Engineering Geology and Hydrogeology*, Geological Society of London, Paper 11-034R

Beavan, J., Fielding, E., Motagh, M., Samsonov, S., & Donnelly, N. (2011). Fault location and slip distribution of the 22 February 2011  $M_w$  6.2 Christchurch, New Zealand, earthquake from geodetic data. *Seismological Research Letters*, 82(6), 789-799.

Beavan, J., Motagh, M., Fielding, E. J., Donnelly, N., & Collett, D. (2012). Fault slip models of the 2010–2011 Canterbury, New Zealand, earthquakes from geodetic data and observations of postseismic ground deformation. *New Zealand Journal of Geology and Geophysics*, 55(3), 207-221.

Berryman, K. R., Cochran, U. A., Clark, K. J., Biasi, G. P., Langridge, R. M., & Villamor, P. (2012). Major earthquakes occur regularly on an isolated plate boundary fault. *Science*, 336(6089), 1690-1693.

Bolt, BA & Herraiz, M 1983, 'Simplified estimation of seismic moment from seismograms', *Bulletin of the Seismological Society of America*, vol. 73, no. 3, pp. 735-48.

Bradley, B. A., Quigley, M. C., Van Dissen, R. J., & Litchfield, N. J. (2014) Ground motion and seismic source aspects of the Canterbury earthquake sequence. *Earthquake Spectra*.

Bradley, B. A. (2012). Strong ground motion characteristics observed in the 4 September 2010 Darfield, New Zealand earthquake. *Soil Dynamics and Earthquake Engineering*, 42, 32-46.

Buech, F, Davies, TR & Pettinga, JR 2010, 'The Little Red Hill Seismic Experimental Study: Topographic Effects on Ground Motion at a Bedrock-Dominated Mountain Edifice', *Bulletin of the Seismological Society of America*, vol. 100, no. 5A, pp. 2219-29. DOI:10.1785/0120090345

Campbell, J, Pettinga, J & Jongens, R 2012, 'The tectonic and structural setting of the 4th September 2010 Darfield (Canterbury) Earthquake sequence, New Zealand', *New Zealand Journal of Geology and Geophysics (Canterbury, New Zealand, 2010-2011 earthquake sequence)*, vol. 55, no. 3, pp. 155-68.

Cox, S. C., Rutter, H. K., Sims, A., Manga, M., Weir, J. J., Ezzy, T., ... & Scott, D. (2012). Hydrological effects of the  $M_w$  7.1 Darfield (Canterbury) earthquake, 4 September 2010, New Zealand. *New Zealand Journal of Geology and Geophysics*, 55(3), 231-247.

Cox, S. C., Menzies, C. D., Sutherland, R., Denys, P. H., Chamberlain, C., & Teagle, D. A. H. (2014). Changes in hot spring temperature and hydrogeology of the Alpine Fault hanging wall, New Zealand, induced by distal South Island earthquakes. *Geofluids*.

Crone, A. J., Machette, M. N., & Bowman, J. R. (1997). Episodic nature of earthquake activity in stable continental regions revealed by palaeoseismicity studies of Australian and North American Quaternary faults. *Australian Journal of Earth Sciences*, 44(2), 203-214.

Cubrinovski, M., Green, R.A., Allen, J., Ashford, S., Bowman, E., Bradley, B., Cox, B., Hutchinson, T., Kavazanjian, E., Orense, R., Pender, M., Quigley, M. and Wotherspoon, L. (2010) Geotechnical Reconnaissance of the 2010 Darfield (Canterbury) Earthquake. *Bulletin of the New Zealand Society for Earthquake Engineering* 43(4): 243-320

De Pascale, G. P., Quigley, M. C., & Davies, T. R. (2014) Lidar reveals uniform Alpine fault offsets and bimodal plate boundary rupture behavior, New Zealand. *Geology*, G35100-1.

Dorn, C, Green, AG, Jongens, R, Carpentier, S, Kaiser, AE, Campbell, F, Horstmeyer, H, Campbell, J, Finnemore, M & Pettinga, J, (2010), High-resolution seismic images of potentially seismogenic structures beneath the northwest Canterbury Plains, New Zealand, *Journal of Geophysical Research B: Solid Earth*, vol. 115, no. 11. DOI:10.1029/2010JB007459

Duffy, B., Campbell, J., Finnemore, M., & Gomez, C. (2014). Defining fault avoidance zones and associated geotechnical properties using MASW: a case study on the Springfield Fault, New Zealand. *Engineering Geology*, 183, 216-229.

Duffy, B., Quigley, M., Van Dissen, R., Stahl, T., Leprince, S., McInnes, C., Barrell, D., Bilderback, E., (2013) Fault kinematics and surface deformation across a releasing bend during the 2010  $M_w$  7.1 Darfield, New Zealand, earthquake revealed by differential LiDAR and cadastral surveying, *GSA Bulletin*

Elliott, J. R., Nissen, E. K., England, P. C., Jackson, J. A., Lamb, S., Li, Z., ... & Parsons, B. (2012). Slip in the 2010–2011 Canterbury earthquakes, New Zealand. *Journal of Geophysical Research: Solid Earth* (1978–2012), 117(B3).

Fry, B., & Gerstenberger, M. C. (2011). Large apparent stresses from the Canterbury earthquakes of 2010 and 2011. *Seismological Research Letters*, 82(6), 833-838.

- Geller, R. J., Jackson, D. D., Kagan, Y. Y., & Mulargia, F. (1997). Enhanced: earthquakes cannot be predicted. *Science*, 275(5306), 1616-1620.
- Geller, R. J. (2011). Shake-up time for Japanese seismology. *Nature*, 472(7344), 407-409.
- Gerstenberger, M., McVerry, G., Rhoades, D., & Stirling, M. (2014). Seismic hazard modeling for the recovery of Christchurch. *Earthquake Spectra*, 30(1), 17-29.
- Gledhill, K., Ristau, J., Reyners, M., Fry, B., & Holden, C. (2011). The Darfield (Canterbury, New Zealand)  $M_w$  7.1 earthquake of September 2010: A preliminary seismological report. *Seismological Research Letters*, 82(3), 378-386.
- Grant, LB, Waggoner, JT, Rockwell, TK & von Stein, C 1997, 'Paleoseismicity of the north branch of the Newport-Inglewood fault zone in Huntington Beach, California, from cone penetrometer test data', *Bulletin of the Seismological Society of America*, vol. 87, no. 2, pp. 277-93.
- Gulley, A. K., Dudley Ward, N. F., Cox, S. C., & Kaipio, J. P. (2013). Groundwater responses to the recent Canterbury earthquakes: a comparison. *Journal of Hydrology*, 504, 171-181.
- Hatton, JW, Black, JC & Foster, PF 1987, 'New Zealand's Clyde Power Station', *International Water Power and Dam Construction*, vol. 39, no. 12, pp. 15-20.
- Heron, D, Lukovic, B, Massey, C, Ries, W & McSaveney, M 2014, 'GIS modelling in support of earthquake-induced rockfall and cliff collapse risk assessment in the Port Hills, Christchurch', *Journal of Spatial Science*, vol. 59, no. 2, pp. 313-32.
- Hillis, R., Sandiford, M., Reynolds, S., Quigley, M. (2008) Present-Day Stresses, Seismicity and Neogene-Recent Tectonics of Australia's 'Passive' Margins: Intraplate Deformation Controlled by Plate Boundary Forces, In: Johnson, H., Dore, A., Gatliff, R.W., Holdsworth, R., Lundin, E.R., Ritchie, J.D. (eds) *The Nature and Origin of Compression in Passive Margins*, Geological Society of London, Special Publications 306, 71-90. DOI: 10.1144/SP306.3
- Hornblow, S., Quigley, M., Nicol, A., Van Dissen, R., Wang, N. (2014) Paleoseismology of the 2010  $M_w$  7.1 Darfield (Canterbury) earthquake source, Greendale Fault, New Zealand, *Tectonophysics*, in press
- Holden, C., Beavan, J., Fry, B., Reyners, M., Ristau, J., Van Dissen, R., Villamor, P., Quigley, M., 2011, Preliminary source model of the  $M_w$  7.1 Darfield earthquake from geological, geodetic and seismic data, *Proceedings of the Ninth Pacific Conference on Earthquake Engineering Building an Earthquake-Resilient Society 14-16 April, 2011, Auckland, New Zealand*, Paper 164, 7p.
- Holzer, T. L., & Savage, J. C. (2013). Global earthquake fatalities and population. *Earthquake Spectra*, 29(1), 155-175.
- Honegger, D. G., Nyman, D. J., Johnson, E. R., Cluff, L. S., & Sorensen, S. P. (2004). Trans-Alaska pipeline system performance in the 2002 Denali fault, Alaska, earthquake. *Earthquake spectra*, 20(3), 707-738.
- Hughes, M., Quigley, M., van Ballegooy, S., Deam, B., Bradley, B, Hart, D., Measures, R., (2015) The sinking city: Earthquakes increase flood hazard in Christchurch, New Zealand, *GSA Today*, in press

Ito, T., Ozawa, K., Watanabe, T., & Sagiya, T. (2011). Slip distribution of the 2011 off the Pacific coast of Tohoku Earthquake inferred from geodetic data. *Earth, planets and space*, 63(7), 627-630.

Johnston, A. C. (1989). The seismicity of 'stable continental interiors'. In *Earthquakes at North-Atlantic Passive Margins: Neotectonics and Postglacial Rebound* (pp. 299-327). Springer Netherlands.

Jonsson, S., H. Zebker, P. Segall, and F. Amelung. 2002. Fault slip distribution of the 1999  $M_w$  7.1 Hector Mine, California, earthquake, estimated from satellite radar and GPS measurements. *Bull. Seis. Soc. Am* 92 (4):1377-1389.

Jordan, T. H., Chen, Y. T., Gasparini, P., Madariaga, R., Main, I., Marzocchi, W., ... & Zschau, J. (2011). Operational earthquake forecasting. State of knowledge and guidelines for utilization. *Annals of Geophysics*, 54(4).

Kaiser, A., and 23 others (2012). The  $M_w$  6.2 Christchurch earthquake of February 2011: preliminary report. *New Zealand journal of geology and geophysics*, 55(1), 67-90.

Kanamori, H., & Brodsky, E. E. (2004). The physics of earthquakes. *Reports on Progress in Physics*, 67(8), 1429.

Kerr, J. et al (2003) Planning for development of land on or close to active faults: a guideline to assist resource management planners in New Zealand, Ministry for the Environment, ME number 565: 67 p.

Kennett, BLN 2002, *The Seismic Wavefield: Volume 1. Introduction and Theoretical Development*, Cambridge University Press, Cambridge.

Khajavi, N., Quigley, M., McColl, S.T. and Rezanejad, A. (2012) Seismically-induced boulder displacement in the Port Hills, New Zealand during the 2010 Darfield (Canterbury) earthquake. *New Zealand Journal of Geology and Geophysics*, Vol. 55, No. 3, p. 271-278

Khajavi, N., Quigley, M., Langridge, R., (2014) Influence of topography and basement depth on surface rupture morphology revealed from LiDAR and field mapping, Hope Fault, New Zealand, *Tectonophysics*

Kilb, D., Gomberg, J., & Bodin, P. (2000). Triggering of earthquake aftershocks by dynamic stresses. *Nature*, 408(6812), 570-574.

King, G. C., Stein, R. S., & Lin, J. (1994). Static stress changes and the triggering of earthquakes. *Bulletin of the Seismological Society of America*, 84(3), 935-953.

Li, Y-G., De Pascale, G., Quigley, M., Gravely, D., (2014) Fault Damage Zones of the M7.1 Darfield and M6.3 Christchurch Earthquake Sources Viewed with Fault-Zone Trapped Waves, *Tectonophysics* 618, 79-101

Litchfield, N. J.; Van Dissen, R. J.; Hornblow, S.; Quigley, M.; Archibald, G. (2014) Detailed analysis of Greendale Fault ground surface rupture displacements and geometries, GNS Science Report 2013/18. 166 p.

- Mackey, B., and Quigley, M., (2014) Strong proximal earthquakes revealed by cosmogenic  $^3\text{He}$  dating of prehistoric rockfalls, Christchurch, New Zealand, *Geology*
- Marano, K. D., Wald, D. J., & Allen, T. I. (2010). Global earthquake casualties due to secondary effects: a quantitative analysis for improving rapid loss analyses. *Natural Hazards*, 52(2), 319-328.
- Massey, C. I., McSaveney, M. J., Taig, T., Richards, L., Litchfield, N. J., Rhoades, D. A., ... & Van Dissen, R. J. (2014). Determining rockfall risk in Christchurch using rockfalls triggered by the 2010-2011 Canterbury earthquake sequence. *Earthquake Spectra*, 30(1), 155-181.
- Norris, R. J., & Cooper, A. F. (2001). Late Quaternary slip rates and slip partitioning on the Alpine Fault, New Zealand. *Journal of Structural Geology*, 23(2), 507-520.
- Pettinga, J. R., Yetton, M. D., Van Dissen, R. J., & Downes, G. (2001). Earthquake source identification and characterisation for the Canterbury region, South Island, New Zealand. *Bulletin of the New Zealand National Society for Earthquake Engineering*, 34(4), 282-317.
- Pirrotta, C, Barbano, MS, Guarnieri, P & Gerardi, F 2007, 'A new dataset and empirical relationships between magnitude/intensity and epicentral distance for liquefaction in central-eastern Sicily', *Annals of Geophysics*, vol. 50, no. 6, pp. 763-74. DOI:10.4401/ag-3055
- Price, E. J., & Bürgmann, R. (2002). Interactions between the Landers and Hector Mine, California, earthquakes from space geodesy, boundary element modeling, and time-dependent friction. *Bulletin of the Seismological Society of America*, 92(4), 1450-1469.
- Quigley, M., Van Dissen, R., Villamor, P., Litchfield, N., Barrell, D., Furlong, K., Stahl, T., Duffy, B., Bilderback, E., Noble, D., Townsend, D., Begg, J., Jongens, R., Ries, W., Claridge, J., Klahn, A., Mackenzie, H., Smith, A., Hornblow, S., Nicol, R., Cox, S., Langridge, R., Pedley, K., (2010a), Surface rupture of the Greendale Fault during the  $M_w$  7.1 Darfield (Canterbury) earthquake, New Zealand: Initial Findings, *New Zealand Society for Earthquake Engineering Bulletin*, December Special volume, Preliminary Assessment of Initial Observations of the Darfield [Canterbury] Earthquake Sequence
- Quigley, M., Villamor, P., Furlong, K., Beavan, J., Van Dissen, R., Litchfield, N., Stahl, T., Duffy, B., Bilderback, E., Noble, D., Barrell, D., Jongens, R., Cox, S., (2010b) Previously Unknown Fault Shakes New Zealand's South Island, *Eos, Transactions, American Geophysical Union*, Vol. 91, No. 49, p.469-471
- Quigley, M., Van Dissen, R., Litchfield, N., Villamor, P., Duffy, B., Barrell, D., Furlong, K., Stahl, T., Bilderback, E., Noble, D. (2012) Surface rupture during the 2010  $M_w$  7.1 Darfield (Canterbury, New Zealand) earthquake: implications for fault rupture dynamics and seismic-hazard analysis, *Geology* 40 (1) p. 55-59.
- Quigley, M., Bastin, S., and Bradley, B., (2013) Recurrent liquefaction in Christchurch, New Zealand during the Canterbury earthquake sequence, *Geology* 41 (4) p. 419-422.
- Quigley, M., Cupper, M., Sandiford, M. (2006) Quaternary faults of south-central Australia: palaeoseismicity, slip rates and origin, *Australian Journal of Earth Sciences*, 53, 285-30

- Quigley, M., Sandiford, M., Alimanovic, A., Fifield, L.K. (2007a) Landscape responses to intraplate tectonism: quantitative constraints from  $^{10}\text{Be}$  abundances, *Earth and Planetary Science Letters*, 261, 120-133, doi:10.1016/j.epsl.2007.06.020
- Quigley, M., Sandiford, M., Fifield, K., Alimanovic A. (2007b) Bedrock erosion and relief production in the northern Flinders Ranges, Australia, *Earth Surface Processes and Landforms*, 32, 929-944, doi: 10.1002/esp.1459
- Quigley, M., Clark, D., Sandiford, M. (2010) Tectonic geomorphology of Australia, In: Geological Society London Special Publication 'Australian landscapes' ; v. 346; p. 243-265 doi:10.1144/SP346.13
- Reid, H. F. (1910), *The California Earthquake of April 18, 1906*, Carnegie Institution of Washington, Washington, D. C.
- Robinson, TR & Davies, TRH 2013, 'Review Article: Potential geomorphic consequences of a future great ( $M_w = 8.0+$ ) Alpine Fault earthquake, South Island, New Zealand', *Natural Hazards and Earth System Sciences*, vol. 13, pp. 2279–99. DOI:10.5194/nhess-13-2279-2013
- Salichon, J., P. Lundgren, B. Delouis, and D. Giardini. 2004. Slip History of the 16 October 1999  $M_w$  7.1 Hector Mine Earthquake (California) from the Inversion of InSAR, GPS, and Teleseismic Data. *Bull. Seis. Soc. Am.*, 94, 2015-2027.
- Scholz, C. H. (2002). *The mechanics of earthquakes and faulting*. Cambridge university press.
- Shcherbakov, R., Nguyen, M. and Quigley, M. (2012) Statistical Analysis of the 2010  $M_w$  7.1 Darfield Earthquake Aftershock Sequence. *New Zealand Journal of Geology and Geophysics*, Vol. 55, No. 3, p. 305-311
- Stahl, T., Bilderback, E., Quigley, M., Nobes, D., Massey, C., (2014) Coseismic landsliding during the  $M_w$  7.1 Darfield (Canterbury) earthquake: implications for the paleoseismic studies of landslides, *Geomorphology*.
- Steady, S., Jiménez, A., & Holden, C. (2013). Stress triggering and the Canterbury earthquake sequence. *Geophysical Journal International*, ggt380.
- Stirling, MW, Anooshehpour, A, Brune, JN, Biasi, GP & Wesnousky, SG 2002, 'Assessment of the Site Conditions of Precariously Balanced Rocks in the Mojave Desert, Southern California', *Bulletin of the Seismological Society of America*, vol. 92, no. 6, pp. 2139-44. DOI:10.1785/0120010221
- Stirling, M, Goded, T, Berryman, K & Litchfield, N 2013, 'Selection of Earthquake Scaling Relationships for Seismic-Hazard Analysis', *Bulletin of the Seismological Society of America*, vol. 103, no. 6, pp. 2993-3011. DOI:10.1785/0120130052
- Twiss, R. J., & Moores, E. M. (2001). *Structural Geology*. 2nd edition. Freeman. New York, 736 p.
- Van Dissen, R., Hornblow, S., Quigley, M., Litchfield, N., Villamor, P., Nicol, A., (2013) Towards the development of design curves for characterising distributed strike-slip surface fault rupture displacement: an example from the 4 September, 2010, Greendale Fault rupture, NZ, *Proc. 19th NZGS Geotechnical Symposium*, 8 p.

Van Dissen, R., D. Barrell, N. Litchfield, P. Villamor, M. Quigley, A. King, K. Furlong, J. Begg, D. Townsend, H. Mackenzie, T. Stahl, D. Noble, B. Duffy, E. Bilderback, J. Claridge, A. Klahn, R. Jongens, S. Cox, R. Langridge, W. Ries, R. Dhakal, A. Smith, S. Hornblow, R. Nicol, K. Pedley, H. Henham, R. Hunter, A. Zajac, T. Mote (2011) Surface rupture displacement on the Greendale Fault during the  $M_w$  7.1 Darfield (Canterbury) earthquake, New Zealand, and its impact on man-made structures, Proceedings of the Ninth Pacific Conference on Earthquake Engineering: Building an Earthquake-Resilient Society, Auckland, New Zealand

Villamor, P., Litchfield, N., Barrell, D., Van Dissen, R., Hornblow, S., Quigley, M., Levick, S., Ries, W., Duffy, B., Begg, J., Townsend, D., Stahl, T., Bilderback, E., Noble, D., Furlong, K. and Grant, H. (2012) Map of the 2010 Greendale Fault surface rupture, Canterbury, New Zealand: Application to land use planning. *New Zealand Journal of Geology and Geophysics*, Vol. 55, No. 3, p. 223-230

Volkwein, A, Labiouse, V & Schellenberg, K 2011, 'Summary on the NHSS Special Issue "Rockfall protection – from hazard identification to mitigation measures"', *Natural Hazards and Earth System Science*, vol. 11, pp. 2727-8. DOI:10.5194/nhess-11-2727-2011

Wallace, L. M., Beavan, J., McCaffrey, R., Berryman, K., & Denys, P. (2007). Balancing the plate motion budget in the South Island, New Zealand using GPS, geological and seismological data. *Geophysical Journal International*, 168(1), 332-352.

Wesnousky, S. G. (2008). Displacement and geometrical characteristics of earthquake surface ruptures: Issues and implications for seismic-hazard analysis and the process of earthquake rupture. *Bulletin of the Seismological Society of America*, 98(4), 1609-1632.